UPPSALA UNIVERSITET

Examensarbete vid Institutionen för geovetenskaper
Degree Project at the Department of Earth Sciences
ISSN 1650-6553 Nr 550

Some Like It Hot: Pre-heating Prior to Bioreactor Treatment Enhances Nitrogen Removal From Mine Drainage

Vissa gillar det varmt: Förvärmning före bioreaktor-behandling förbättrar kväverening av gruvlakvatten

Laura Nina Bettoni

INSTITUTIONEN FÖR GEOVETENSKAPER
DEPARTMENT OF EARTH SCIENCES

Examensarbete vid Institutionen för geovetenskaper
Degree Project at the Department of Earth Sciences
ISSN 1650-6553 Nr 550

Some Like It Hot: Pre-heating Prior to Bioreactor Treatment Enhances Nitrogen Removal From Mine Drainage

Vissa gillar det varmt: Förvärmning före bioreaktor-behandling förbättrar kväverening av gruvlakvatten

Laura Nina Bettoni

The work for this thesis was carried out in cooperation with LKAB.

Title page: picture of the denitrifying woodchip bioreactor taken by the author during field work.

ISSN 1650-6553

Published at Department of Earth Sciences, Uppsala University (www.geo.uu.se), Uppsala, 2022

Abstract

Some Like It Hot: Pre-heating Prior to Bioreactor Treatment Enhances Nitrogen Removal From Mine Drainage

Laura Nina Bettoni

Ammonium-nitrate based explosives (NH_4NO_3) used within the operations of Kiruna iron ore mine release nitrate (NO_3^-) into the environment, potentially having adverse effects on local river-systems. One way of reducing NO_3^- impacts to the environment is through a woodchip denitrifying bioreactor (DBR). Waste rock leachate is collected and passed through the bioreactor, where denitrifying microbial communities reduce NO_3^- to nitrogen gas (N_2) using a carbon energy source. However, the efficiency of the DBR present in Kiruna iron ore mine has declined since the start of its operation leading to lower values of NO_3^-removal throughout the years.

Denitrification being a temperature dependent process, a heating device was installed to warm up the water prior to the DBR treatment to counterbalance this decrease. The effect of which has been assessed within this thesis. Chemical analyses encompassing NO_3^-, nitrite (NO_2^-), ammonium (NH_4^+), total organic carbon (TOC), phosphorus compounds (tot-P, PO_4-P), and bacterial abundance were then investigated along a flowpath in the DBR. Overall, the results have shown that with an increase in temperature prior to the treatment, TOC, tot-P, PO_4-P release was improved. Moreover, NO_3^- removal doubled compared to the previous year. TOC, tot-P and PO_4-P are the result of the hydrolysis process, transforming the woodchips in available carbon source and providing nutrients for the bacteria to perform denitrification. Similarly, the bacterial abundance presented a significant increase with temperature. This suggest that both hydrolysis and bacteria growth enhancement with temperature ultimately participated in the improvement of the denitrification reaction. Moreover, a long-lasting effect of temperature on NO_3^- removal was observed during a following cold period as NO_3^- removal stayed above 45% after two months without heating. It is suggested that the cost of heating can be reduced by inducing "heat pulse" instead of continuous heating. Adding a heating system prior to treatment represents a promising solution for the future of sustainable mining, particularly for mines located in extreme climates such as Kiruna.

Keywords: denitrification, nitrate removal, temperature, woodchip bioreactor, waste rock leachate.

Degree Project E1 in Earth Science, 1GV025, 30 credits
Supervisor: Roger Herbert
Department of Earth Sciences, Uppsala University, Villavägen 16, SE-752 36 Uppsala (www.geo.uu.se)

ISSN 1650-6553, Examensarbete vid institutionen för geovetenskaper, No. 550, 2022

The whole document is available at www.diva-portal.org

Popular science summary

Some Like It Hot: Pre-heating Prior to Bioreactor Treatment Enhances Nitrogen Removal From Mine Drainage

Laura Nina Bettoni

The Kiruna mine, operated for decades by the LKAB (Luossavaara-Kiirunavaara Aktiebolag) mining company, hosts precious treasure trapped within the rock: iron ore. To free it, ammonium and nitrate-based explosives are detonated in the many underground galleries of the mine.
Good news: this method works.
Bad news: nitrogen compounds released from the mine can impact the quality of surrounding waters.

Explosives that do not detonate accumulate in the waste rock, where, in contact with water, they dissociate and dissolve, mainly in the form of nitrate. Nitrate is defined by the chemical formula NO_3^- and can, in large quantities, be detrimental for aquatic ecosystems. As a result, LKAB has investigated the use of woodchips bioreactors to protect the environment.

The process dominating the treatment within the woodchip bioreactor is called denitrification. It is a reaction dominated by bacteria which, when deprived of oxygen, will use the oxygen atoms present in the nitrate and release nitrogen (N_2 is a harmless gas making up 78% of the atmosphere). However, this treatment has limitations. First, for denitrification to be effective, bacteria need energy. As for us humans who consume food as energy, bacteria consume a source of carbon (e.g., glucose that is released from woodchips). For this source to be available and consumed, woodchips must first be degraded. This process is called hydrolysis.

Many factors influence the efficiency of a bioreactor, but this project focused on one factor specifically: temperature. Since the start of its operation, the Kiruna bioreactor has lost its efficiency in removing nitrate. To counterbalance this effect, a heating system was installed to heat the water prior to the denitrification treatment since denitrification is temperature dependent.

The results were conclusive. The nitrate removal rate improved by more than half compared to the previous year. In addition, it has been shown that an increase in temperature induced an increase in the release of organic carbon from the woodchips (due to better hydrolysis) as well as growth in the bacterial community. Both these effects imply a positive effect on denitrification. A long-lasting effect of temperature on nitrate removal has also been found two months after heating was turned off where nitrate removal stayed up to 45%. This would suggest that heating the water by heat pulse would result in similar results and in turn would reduce operating costs. As such, these conclusions have been promising for the future of sustainable mining for mines located in extreme climates such as Kiruna.

Keywords: denitrification, nitrate removal, temperature, woodchip bioreactor, waste rock leachate.

Degree Project E1 in Earth Science, 1GV025, 30 credits
Supervisor: Roger Herbert
Department of Earth Sciences, Uppsala University, Villavägen 16, SE-752 36 Uppsala (www.geo.uu.se)

ISSN 1650-6553, Examensarbete vid institutionen för geovetenskaper, No. 550, 2022

The whole document is available at www.diva-portal.org

Table of Contents

1 Introduction

Ammonium nitrate (NH_4NO_3) is widely used as a base for explosives in the mining industry (Forsyth et al. 1995). However, up to 28% of the explosives used remain undetonated and accumulate on the excavated rock (Häyrynen et al. 2009; Morin & Hutt 2009). Being highly soluble in water, NH_4NO_3 tends to dissolve, primarily in the form of nitrate (NO_3^-), in rainfall and snowmelt that infiltrate into the waste rock (Clark 1981). Nitrate is then carried within the mining drainage system into nearby surface water and groundwater. When present in large quantities, NO_3^- can prove detrimental for the environment. An excess release could result in acidification, eutrophication and hypoxia leading to habitat degradation and biodiversity losses in the receiving water bodies (Halling-Sørensen & Jorgensen 1993; Stumm & Morgan 2012).

Nitrate released from the use of explosives is an issue faced by mines around the world (Zaitsev et al. 2008; Häyrynen et al. 2009; Bailey et al. 2013; Kiani et al. 2022). Kiruna iron ore mine, which has been using NH_4NO_3 explosive resource for years, is no exception (Herbert et al. 2014). As a result, an elevated NO_3^- concentration is present in both the mine and its process waters, which are eventually released into the environment (LKAB 2016; Nordström & Herbert 2019). Therefore, to minimize further contamination, the Luossavaara-Kiirunavaara Aktiebolag (LKAB) mining company, which is responsible for the mining operations within the Kiruna mine, has constructed a treatment system consisting of three woodchips denitrifying bioreactors (DBR). These were constructed under the EIT RawMaterial project called NITREM with the goal of minimizing the concentration of NO_3^- in the leachate from the mining waste rock deposit before release (NITREM n.d.).

DBR have been implemented for several decades as an emerging biotechnology to reduce NO_3^- concentrations in agricultural drainage systems (Christianson et al. 2013; Addy et al. 2016; Feyereisen et al. 2016). Having low construction and operational costs and having a comparatively long lifespan of up to 15 years (Schipper et al. 2010) the interest in such a technique has grown in recent years and has expanded into the mining industry (Zaitsev et al. 2008; Nordström & Herbert 2019). A DBR is a subsurface system where denitrification by micro-organisms utilizing a carbon source (such as, for example, glucose $C_6H_{12}O_6$), reduces the NO_3^- into a harmless nitrogen gas (N_2), as seen in the net denitrification reaction (1) (Nordström & Herbert 2018). Apart from N_2, bicarbonate (HCO_3^-), carbonic acid (H_2CO_3) and water (H_2O) are released, with HCO_3^- having the effect of increasing the buffering capacity of the water (Ibanez et al. 2008).

$$\mathbf{NO_3}^- + \frac{5}{24}C_6H_{12}O_6 \rightarrow \frac{1}{2}\,\mathbf{N_2} + HCO_3^- + \frac{1}{4}H_2CO_3 + \frac{1}{2}H_2O \qquad (1)$$

Denitrification rates, defining the bioreactor efficiency, are affected by several parameters such as carbon availability, microbial communities, water chemistry and temperature (Nordström & Herbert 2019; Maxwell et al. 2020). If the environmental conditions do not support complete denitrification, rates will be reduced and may result in the production of by-products such as nitrite (NO_2^-), ammonium (NH_4^+) and nitrous oxide (N_2O) which in turn could be harmful for the environment (Nordström & Herbert 2018; Davis et al. 2019; Nordström et al. 2021). Therefore, it is important to understand the processes that impact bioreactor performance.

This thesis will primarily focus on the effects of temperature on NO_3^- removal in a woodchip denitrifying bioreactor. In Kiruna, the water temperature flowing within the bioreactor is consistently between 1 and 6°C with the lowest temperature at the end of the winter and the highest during the summer season (Herbert 2019, 2022). Denitrification, being a microbial process, is enhanced by an increase in temperature which promotes microbial growth (Schipper et al. 2014; Maxwell et al. 2020). Since the beginning of the NITREM project, a decline in the bioreactors treatment efficiency has been observed (Herbert 2022). Therefore, warming up the water before treatment was thought to represent a solution to enhance the denitrification rate, the effect of which has been assessed in this report.

2 Aims

The aim of this study is to determine if heating of waste rock leachate water, prior to treatment in a denitrifying bioreactor, can enhance denitrification efficiency and, thus, achieve a higher degree of NO_3^- removal. For this purpose, bioreactor water sampling was performed over the thesis period, when the heating was conducted. Chemical analyses were made on several compounds (nitrogen compounds, total organic carbon, phosphorus compounds, and sulfate) and the bacterial community was quantified. These results were then assessed and compared to previous analyses that were made available through the NITREM project.

Based on the data, the relationship between NO_3^- removal rate and temperature has been investigated, and a simple regression model has been established between these two parameters. Additionally, the relationship between temperature changes, bacterial growth, and total organic carbon and phosphorus compounds has been examined. Finally, the economic aspect of the project has been assessed to evaluate potential solutions to using a heating system while remaining cost-effective.

3 Background

3.1 The biological nitrogen cycle

Nitrogen (N) is one of the main elements present within living organisms. However, its gas form (N_2), which represents 79% of the atmosphere, cannot be used by most living organisms and must be transformed (Trenberth & Guillemot 1994; Bothe et al. 2006; Schlesinger & Bernhardt 2020). For that purpose, it can undergo a variety of oxidation and reduction (redox) reactions controlled by different kind of organisms (bacteria, archaea, fungi) which describe the biological N-cycle (Bothe et al. 2006). The common pathways included in this cycle are nitrogen fixation, nitrification, dissimilatory reduction of NO_3^-/ NO_2^- to NH_4^+ (DNRA), denitrification and anaerobic NH_4^+ oxidation (anammox) (figure 1). All of these processes are governed by specific organisms which use these reactions to gain energy (Bothe et al. 2006).

Nitrogen fixation refers to the process during which nitrogen gas (N_2) is reduced to NH_4^+, a major inorganic nitrogen source for plants (Liu & von Wirén 2017). When the plants die, NH_4^+ is returned to the environment as seen with the organic N arrow in figure 1. During nitrification, under aerobic environment conditions, NH_4^+ is biologically oxidized into NO_2^- and ultimately into NO_3^-. Reversely, under anaerobic conditions, NO_3^- is reduced to NO_2^- and further into NH_4^+ or N_2 by either DNRA or denitrification reactions, respectively. Anammox is also a pathway to reduce $NO_3^-$to N_2, through the utilization of an NH_4^+ source (Shiskowski & Mavinic 1998; Bothe et al. 2006; Canfield et al. 2010; Ni & Zhang 2013).

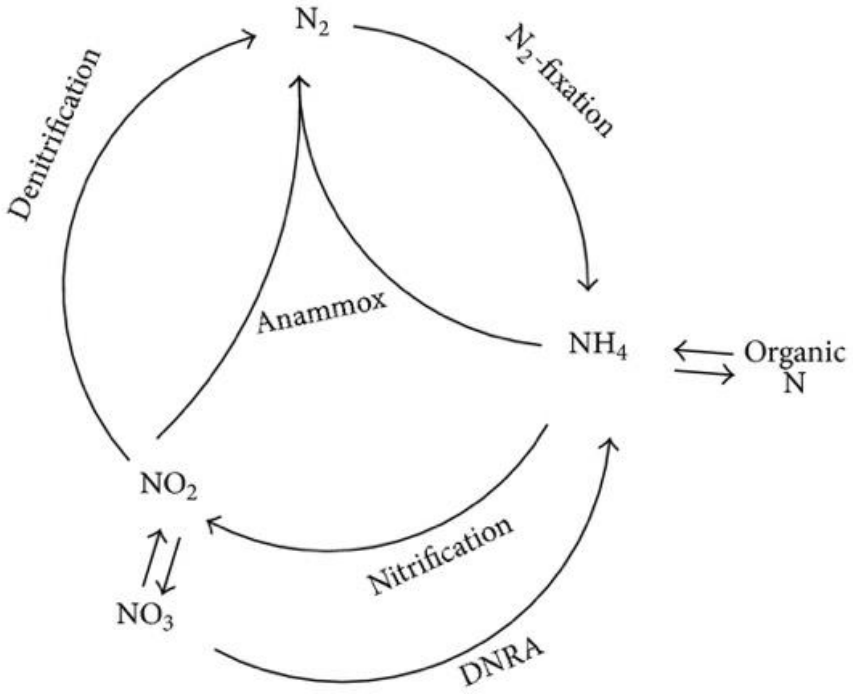

Figure 1. Biological N-cycle (Ni & Zhang 2013)

Environmental conditions are the main parameters that promote one pathway over the other. In anaerobic environments, a large availability of electron donors (e.g., total organic carbon (TOC)) in the system relative to NO_3^-/NO_2^- make DNRA the preferential pathway (Burgin and Hamilton, 2007). In contrast, denitrification would be achieved in an environment where there is a moderate availability of electron donors while anammox would result from an environment with low availability of electron donors (Bothe et al. 2006; Burgin & Hamilton 2007). Nordström et al. (2021) have observed that DNRA gene abundance has a strong positive correlation with both TOC/NO_3^- ratio and temperature. This agrees with the previous statement about the availability of electron donors and other studies which further explain that the relative increase in the DNRA rate is greater than the denitrification following an increase in temperature. Thus, DNRA outcompetes the denitrification process under limited NO_3^- availability in these systems (Rahman et al. 2019; Pandey et al. 2020).

Denitrification and anammox reactions are the main processes resulting in the transformation of NO_3^- into nitrogen gas. However, with NO_3^- dominating the mine waters, denitrification would be the most preferable pathway for NO_3^- removal (Nordström & Herbert 2018).

3.1.1 Denitrification

As stated in the previous section, denitrification reduces NO_3^- to NO_2^- and ultimately to nitrogen gas (N_2) utilizing organic matter (such as glucose) as electron donors. During this process, under anaerobic conditions, organisms (generally bacteria) utilize NO_3^- instead of oxygen as respiratory electron acceptors (Ni and Zhang, 2013). The net denitrification (reaction 1) is accomplished in different reduction steps (reaction 2) (Nordström & Herbert 2018). Where NO stands for nitric oxide and N_2O for nitrous oxide. Each of the resulting NOx reductions are performed by a specialized reductase (enzyme performing reduction) as seen in reaction 2.1-2.4 (Zumft 1997).

$$\boldsymbol{NO_3}^- + \frac{1}{12} C_6H_{12}O_6 \rightarrow \boldsymbol{NO_2}^- + \frac{1}{2} H_2CO_3 \qquad (2.1)$$

Nitrate reductases

$$\boldsymbol{NO_2}^- + \frac{1}{24} C_6H_{12}O_6 + \frac{3}{4} H_2CO_3 \rightarrow \boldsymbol{NO} + HCO_3^- + \frac{1}{2} H_2O \qquad (2.2)$$

Nitrite reductases

$$\boldsymbol{NO} + \frac{1}{24} C_6H_{12}O_6 \rightarrow \frac{1}{2}\boldsymbol{N_2O} + \frac{1}{2} H_2CO_3 \qquad (2.3)$$

Nitric oxide reductases

$$\frac{1}{2}\boldsymbol{N_2O} + \frac{1}{24} C_6H_{12}O_6 \rightarrow \frac{1}{2}\boldsymbol{N_2} + \frac{1}{4} H_2CO_3 \qquad (2.4)$$

Nitrous oxide reductases

In a water-saturated woodchip system, the carbon and energy source provides ideal conditions for the growth of denitrifiers (denitrifying bacteria) which is then promoted against other types of bacteria (Warneke et al. 2011). However, a competition between the different denitrifying communities can affect denitrification. Indeed, an unbalanced concentration of NO_3^- and NO_2^- reductases could lead to an accumulation of NO_2^- in the system (see reaction 2) (Wilderer et al. 1987).

3.2 Processes and factors controlling DBR

DBR are driven by several biogeochemical processes and factors that impact their performances through time. These main factors are summarized in the sections below.

3.2.1 Organic carbon availability and phosphorus

Among the different carbon substrates, woodchips have been preferentially utilized, as they have been found to provide ideal conditions for denitrifying bacteria allowing great NO_3^- removal over time while limiting adverse effects like the emission of by-products such as nitrous oxide (Robertson 2010; Warneke et al. 2011).

Woodchips are primarily composed of carbon, especially cellulose at approximately 45% of the total biomass (Asghari & Yoshida 2010; Chandrasekaran et al. 2012). Cellulose is a complex organic matter that must first be solubilized through hydrolysis to be consumed by bacteria (Iranmahboob et al. 2002). Thereby, the supply of available organic carbon substrate (such as glucose $C_6H_{12}O_6$) for denitrifiers is dependent on the rate of cellulose hydrolysis in the bioreactor (Iranmahboob et al. 2002; Nordström & Herbert 2018). The reaction conditions that affect the enzymatic hydrolysis rate of cellulose are governed by temperature and pH (Sun & Cheng 2002).

A positive correlation between carbon availability and NO_3^- removal rates has been observed in several studies (Schipper et al. 2010; Warneke et al. 2011; Ghane et al. 2015; Nordström & Herbert 2019). However, as the carbon source is being consumed by the bacterial communities through time, the general removal efficiency decreases (Robertson 2010).

Phosphorus is an essential element for the metabolism and growth of denitrifying bacteria with phosphate being a major microbial nutrient (Hunter 2003). DBR represent both sources and sinks for phosphorus compounds. An important source of phosphorus is woodchips leaching, mainly at the startup of the DBR (Healy et al. 2012; Sharrer et al. 2016). Another potential source of phosphate release is, as for organic carbon, hydrolysis which leads to the release of soluble phosphate from the biomass (Ng & Kim 2007).

3.2.2 Preferential flow

In an ideal situation, flow velocity is supposed to be uniform and cover all the pores present in the DBR. However, in reality, it is rarely the case and the flow might be following a specific pathway where the water travels along the path with least resistance (Gerke 2006; Nordström 2019). As a result, the water velocity is non-uniformly distributed. The areas that are not included in this pathway will not contribute to the denitrification process which in turn would decrease NO_3^- removal rates, and thus, the bioreactor efficiency (Cameron & Schipper 2010; Nordström 2019).

3.2.3 Temperature

Temperature dependence on NO_3^- removal rates within DBR are not fully understood and represents the focus of this thesis. Reaction rates are well known to be positively correlated with temperature. Furthermore, enzymatic reaction rates in soil microbial processes, such as NO_3^- reduction or cellulose hydrolysis, are generally found to be enhanced by an increase in temperature (Sun & Cheng 2002; Addy et al. 2016; Arcus et al. 2016; Maxwell et al. 2020; Nordström et al. 2021). This temperature dependency is commonly explained by the Arrhenius equation (3) where k is the rate constant, A is the pre-exponential factor, Ea is the activation energy for the reaction, R is the universal gas constant and T is the absolute temperature. The activation energy is defined as "the energy barrier over which reactants must "jump" to make the transformation into products" (Schipper et al., 2014). The lower the Ea is, the faster the transformation will take place (Schipper et al. 2014; Arcus et al. 2016). The standard values for denitrification are ranged between 53 and 61 kJ mol^{-1} (Takenaka et al. 2011). However, a value of 23.55 kJ mol^{-1} has been obtained from a model optimized values for denitrification at low temperature conditions when not considering rates limited by low NO_3^- concentrations (Nordström 2014). This equation shows that a linear increase in temperature would result in an exponential increase in rate constant.

$$k = Ae^{\frac{-Ea}{RT}} \qquad (3)$$

Maxwell et al. (2020) demonstrated that the temperature sensitivity of NO_3^- removal rates in DBR increased with age. This relationship would also evolve from a 1st order rate law to a 0th order rate law, where rate is independent of the initial NO_3^- concentration, as the microbial community adapts to their environmental conditions (Ghane et al. 2015; Nordström & Herbert 2019). An nth order rate law is expressed as follow (equation 4):

$$r = k\,[NO_3^-]^n \qquad (4)$$

where r is the NO_3^- removal rate, k is the temperature dependent rate constant (equation 3), $[NO_3^-]$ is NO_3^- concentration and n is the rate order.

Finally, even if denitrification has been defined as a temperature dependent process, it is ultimately limited. According to the micromolecular rate theory (MMRT), when the temperature goes above the temperature optimum value (temperature at which the rate is the highest), NO_3^- reduction rates decline (Schipper et al. 2014; Arcus et al. 2016; Nordström & Herbert 2019).

3.3 Heat transfer occurring in a porous media

In porous media, heat propagates by heat transport with the inflowing water, as well as by conduction (also known as diffusion) and ultimately convection (Prasad et al. 1985; Bear 1988; Kaviany 2012).

The heat present within the inflowing water will propagate through the system. However, depending on the environmental conditions, a certain degree of heat loss could happen. Conduction is a process based on energy transfer that occurs on a microscopic scale. The energy (heat) of vibrating atoms is transferred to its neighboring atoms. It is usually measured with thermal conductivity which define the ability of a material to conduct heat. Heat transfer occurs at a lower rate within a material with lower thermal conductivity than within a material with higher thermal conductivity (Chung & Horton 1987; Bear 1988; Kaviany 2012). Finally, convection is mass transfer which is defined by a "mechanism of thermal energy transport in fluids associated with the actual mass movement of fluids from one region to another" (Bear 1988). As the fluid moves, it carries its own heat with it. Indeed, natural convection is caused by the density difference between the cold and warm waters which will induce the cold dense water to sink and the warm water to rise (Prasad et al. 1985; Bear 1988).

3.4 Study area: Kiruna iron ore mine, Sweden

3.4.1 Site description and LKAB company

Kiruna iron ore mine is located in the subarctic climate of northern Sweden (67°51'N 20°13'S) within Norrbotten County (figure 2). The measured mean air temperature of the study site was -5.8°C during the thesis period.

Since 1890, the mine has been operated by LKAB mining company, one of the main suppliers and business partners to the European steel industry (LKAB 2017). Iron ore is extracted within the side rock from the mine which is then crushed and sorted by dry magnetic separation. While the iron ore undergoes separation and transformation steps before being sold, the resulting waste rock is deposited within the mining site. One of the main deposition areas at the time of this study is the so-called triangle deposit area. It is located north of the mine tailing pond and has a footprint area of 0.56 km^2. The water draining from the waste rock leachate is then conducted to three woodchip denitrifying bioreactors (see section 3.5.2) for treatment before release into the Luossajärvi Lake to further join the Raulta River, the Torne River and ultimately flowing into the Baltic Sea (figure 2).

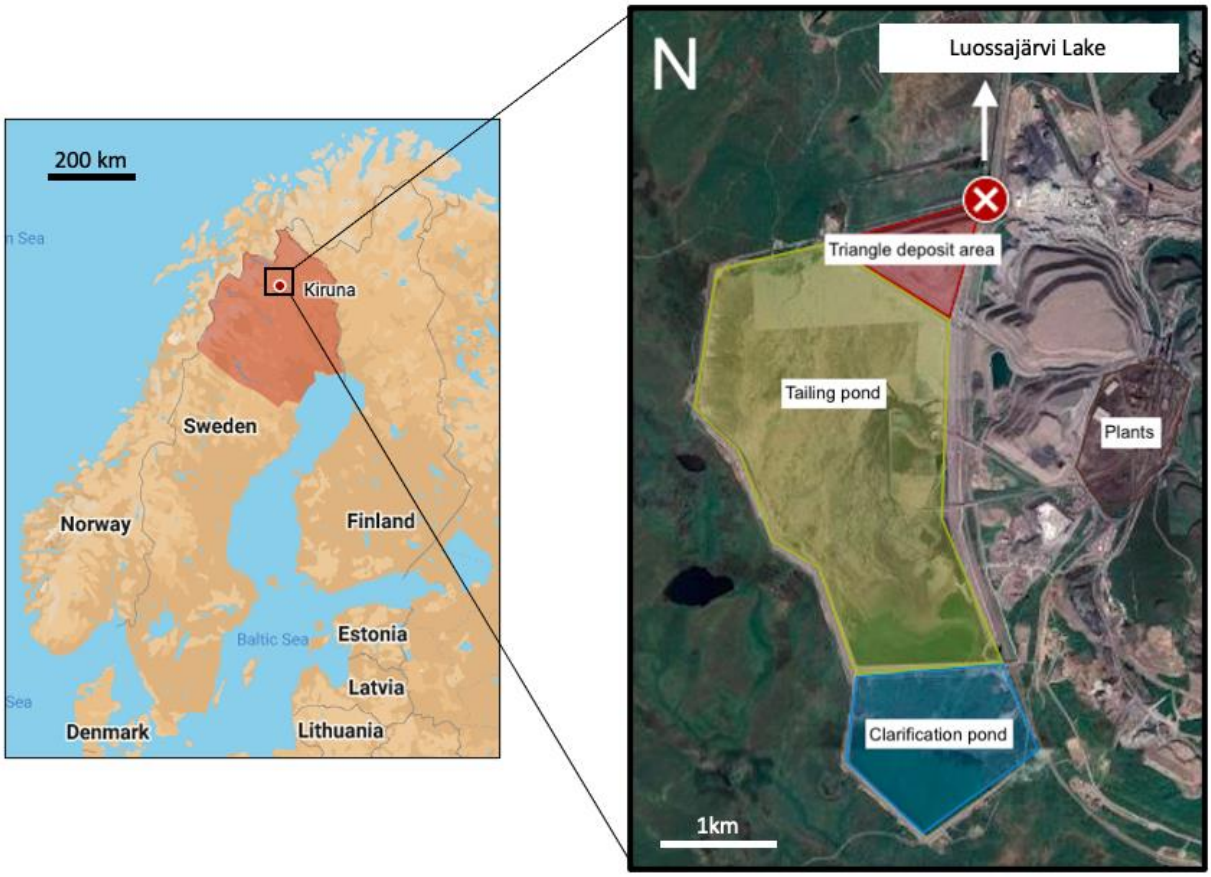

Figure 2. Location of the study site. On the right the cross represents the location of the DBR (edited from *my Google Map*).

3.4.2 NITREM project

NITREM is a project funded by EIT RawMaterials, which has been operating at LKAB since 2018. It has been financially supported by LKAB. The goal of the project was to develop a DBR that would remove NO_3^- from leachate and contribute to the long-term sustainability of waste rock deposition. In total three DBR were constructed; however, this study will only focus on the third one: BR3. It was completed on Monday 17 September 2018 when water first started to flow through the system (NITREM n.d.). From 2018 to 2021, the removal efficiency decreased from 77% to 28% for a total treated water volume of 28450 m^3 during this period (Herbert 2022).

As mentioned before, BR3 is located next to the triangle deposit area (figure 2). The NO_3^- rich leachate is conducted from the triangle deposit area to a groundwater runoff reservoir. From a pumping well, the water is pumped into the bioreactor at the inlet and then released from the outlet on the other side. It is then directed to the mine ditch system before being released into the environment (figure 3.a).

The bioreactor's dimensions are approximately 44 m long, 7 m wide and 2 m deep. The excavation was covered with an impermeable geomembrane and filled with both woodchips, an electron source for denitrification due to their high carbon content and activated sewage sludge (aerated sewage containing

microorganisms such as bacteria). Both a soil cover and inner walls (figure 3.b) were installed to promote the anoxic conditions required for the denitrification process. Their purpose is to force the waters flow deeper into the bioreactor where there is no contact with atmospheric oxygen (Nordström and Herbert, 2018). A layer of protection (geotextile) is placed under the soil cover. In total, 10 PVC tubes placed at 5 different locations in BR3 were installed to allow for water collection (referred to as profile sampling in this report). The water from the bioreactor enters the bottom part of the wells which are perforated within the last 50 cm. These are divided into two categories: A-wells, which are shallower, and B-wells, which are deeper. The DBR inlet is composed of a perforated pipe which distributes the water along the width of the bioreactor. Meanwhile, the DBR outlet is located at the other extremity of the bioreactor (figure 3.b).

BR3 is instrumented with different kinds of permanent sensors, the results of which are continuously available through Process Explorer software on an LKAB server. Permanent temperature sensors are positioned between each profile well. The pumping chamber and the outlet monitoring chamber are equipped with NO_3^- and CTD (electrical conductivity, temperature, water depth) sensors. Discharge is calculated form water depth in the outlet through an ultrasound sensor mounted over the H-flume (figure 3).

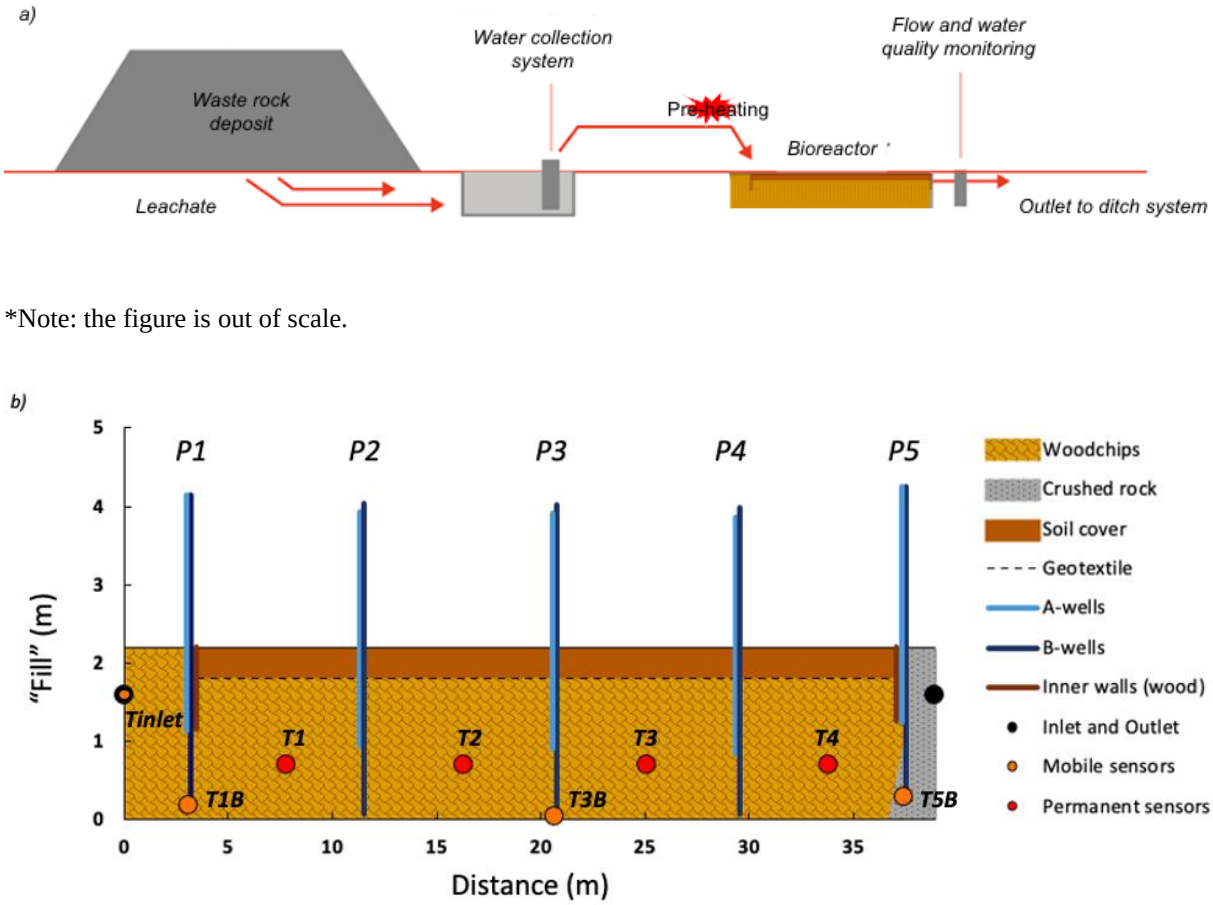

*Note: the figure is out of scale.

Figure 3. Bioreactor cross section with surrounding environment (a) and positions of sampling points and sensors in BR3 (b). Note that the bioreactor, even if represented as a rectangle is in reality trapezoidal (updated and modified from Herbert 2020b; NITREM n.d.).

4 Materials and methods

For study purposes, a heating element was installed before the bioreactor inlet at the beginning of the year 2022 (figure 3.a). Its power capacity was 15 kW and it has proved capable of warming the water up to 30°C before treatment.

The flow, being usually turned off during the winter season, was started again on the 10th of January for a value of 0.10 L s^{-1}. The water was warmed up to 20°C starting the 20th of January which marks the beginning of the experiment. Both flow rate and heating were desired to stay continuous along the study period. Water sampling were performed every week for the inlet and the outlet while a full sampling profile (along the water collection wells, figure 3.b) was done approximately every two weeks. The last profile sampling of the 26th of April marks the end of the experiment.

As mentioned earlier, the aim of this thesis was to assess how temperature could impact denitrification efficiency in a denitrifying woodchip bioreactor. Therefore, temperature along with nitrogen compounds have been the main parameters studied during this period. Other parameters such as flow and electrical conductivity were obtained as they were necessary for the development of the temperature-rate model. Moreover, since denitrification is a biological process, bacterial abundance needed to be analyzed. Total phosphorus (tot-P), dissolved phosphorus (PO_4-P), total organic carbon (TOC) and sulfate (SO_4^{2-}) were investigated to observe processes, apart from denitrification, occurring within the DBR. The energy consumption was measured to evaluate operational cost.

Finally, a range of data had to be collected from both past and present experiments on the bioreactor, with previous data being made available through the NITREM project.

4.1 Temperature

Temperature data was collected by three different methods along the study period (manually, and with permanent, and mobile sensors). Manual measurements were made for each well (including both the inlet and the outlet) for the last three profile episodes. Meanwhile, the sensors were distributed at different distances and depths of the bioreactor and recorded data continuously. In addition to the permanent sensors, four mobile sensors (CTD-Divers, van Essen Instruments, Delft, Netherlands) were installed on the 19th of January to measure temperatures along the bioreactor: at the inlet and in three B-wells (P1B, P3B and P5B) (figure 3.b). Another mobile sensor (Baro-Divers, van Essen Instruments, Delft, Netherlands) was placed outside to measure atmospheric temperature and pressure. These were programmed to measure every 10 minutes and store a mean value every hour. Two temperature loggers (Tinytag Plus 2, Intab, Stenkullen, Sweden) were also installed at the inlet and the outlet of the heater.

For the past profile episodes done before the installation of the heater, the sensors temperatures (T1,T2,T3,T4) were utilized. It is also important to note that since no major temperature differences were observed from one day to another, daily averages were taken from the sensors' measurements to avoid noise. A description of used temperature data can be found in appendix A.

4.1.1 Bioreactor temperature profile

A temperature contour diagram of the bioreactor was made utilizing MATLAB for the last three sampling profiles (29th of March 12th and 26th of April). This was completed by interpolating linearly the temperatures between each measurement's points.

The manual measurements along with the sensors' measurements (T1, T2, T3, T4) with their respective distances and depths were taken as input. This choice was made to cover the maximum area within the bioreactor as A-wells temperatures were only measured manually. B-wells temperature manual measurements were selected instead of the mobile sensors' values for consistency.

4.2 Water sampling

4.2.1 Weekly sampling

Weekly water samples were collected and analyzed for NO_3^- concentrations by LKAB laboratory from both the pumping well and the outlet. The results from the pumping well were assumed similar to the inlet as no clear contamination was detected between these two points. The sampling was performed either with the help of a rope system or a telescopic water sampler. For each position, a 2.5L jar and two 60mL bottles were filled and sent to LKAB laboratory for analysis.

4.2.2 Profile sampling

Approximately every two weeks during the study period, a longitudinal temperature profile along the DBR was conducted (figure 3.b) by myself and LKAB personnel (appendix B). A peristatic pump was used to collect 50mL of sample at each position point along the presumed flowpath in the bioreactor (inlet, wells P1-P5 A/shallow and B/deep, and outlet). The first 1.5-2L of water taken through the pump was disregarded prior to the collection to ensure a representative sample. A picture showing the sampling equipment is shown in figure 4.

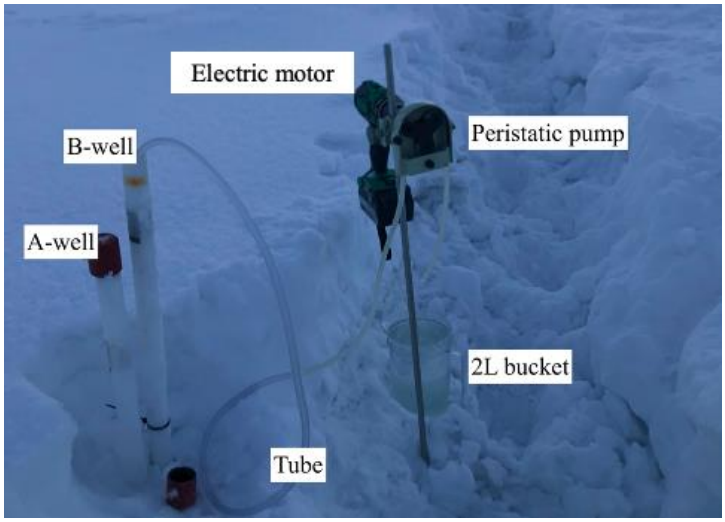

Figure 4. Sampling equipment used for the profile sampling.

4.3 Chemical analyses

4.3.1 Nitrogen compounds

Nitrite (NO_2^-), nitrate (NO_3^-), and ammonium (NH_4^+) were the three main nitrogen species analyzed within this study. Their concentrations were determined using a spectrophotometer instrument (HACH DR1900, portable spectrophotometer) by utilizing adapted reagents testing tubes (HACH-LCK-cuvettes 339 (NO_3^-), 341 (NO_2^-) and 304 (NH_4^+)). After a period of 10 to 15 minutes, the reagents would react with the sample and develop a color which is then measured by the instrument.

Prior to this measurement, the samples for both NO_2^- and NO_3^- testing were diluted 1:11 (1mL of sample for 10mL of deionized water) to fall within detection limit range. The water sample taken at the inlet for NO_2^- testing did not need to be diluted as it is less likely to have NO_2^- at this position. Regarding NH_4^+ testing, no dilution was required as concentration were not expected to be too high according to past analyses done on BR3. The results given by the diluted samples have been multiplied by 11 to give the actual concentration results.

4.3.2 Total phosphorus, dissolved phosphorus, and total organic carbon

Total phosphorus (tot-P), dissolved phosphorus (PO_4-P), and total organic carbon (TOC) underwent analyses for the deeper part of the bioreactor (B-wells) at the Department of Ecology and Genetics, program of Limnology, Uppsala University.

Both tot-P and PO_4-P were measured via spectrophotometry utilizing the molybdenum blue method (Murphy & Riley 1962). However, the preparation of the individual samples differed. For tot-P, persulfate was added before autoclavation to oxidize all the tot-P into PO_4-P, which was then measured by the spectrophotometer. PO_4-P analysis, meanwhile, used filtered samples to remove potential particles containing P. This was done by using a 0.2 µm polyethersulfone syringe filter. To prevent a risk of contaminations of the samples, the first 5mL were put to waste to allow the cleaning of the filter. The filtered samples were then placed into a pre cleaned 50 mL Falcon tube (filled with MQ water for three days).

For TOC, no preparation was needed. 40 mL of sample was taken and analyzed with the Shimadzu TOC-L TNM instrument.

4.3.3 Sulfate

Sulfate (SO_4^{2-}) analysis was used to determine the effects of meltwater on nitrogen compound concentrations during the snowmelt period at the end of the study. It was performed only for the last profile sampling (26th of April). This method is similar to the one used for the nitrogen compounds except that the samples were diluted 1:6 (1mL of sample for 5mL of deionized water) to fall within the analytical range of the method, and adapted reagents test tubes were used (HACH-LCK-cuvettes 153).

4.4 Bacterial abundance

The bacterial abundance analysis was performed for the deeper part of the bioreactor (B-wells). Since it was not possible to perform the analysis directly after the sampling, the samples had to be preserved to prevent an important microbial loss. For this purpose, 10 mL of the samples were mixed with 0.6 mL of sterile-filtered formaldehyde (6% final concentration) and kept in the dark at -20°C until analysis could be properly conducted.

The measurements within this analysis were completed via flow cytometry (CytoFLEX, Beckman Coulter) after staining with SYBR Green I (used as a nucleic acid stain in molecular biology) at a final concentration of 10^{-4} of the stock solution (Lebaron et al. 1998; Gasol & Giorgio 2000). For this purpose, several steps of dilution using Phosphate-Buffered Saline buffered solution (PBS), used in research biology for diluting cells for counting (*PBS* n.d.), were followed (table 1). The blanks were prepared by filtering the original samples through a 0.2µm syringe while the samples were prepared with a courser filter (Whatman glass microfiber GF/C filters). The blanks are used as a comparison for the analysis to determine the background from the actual microbial community.

Table 1. Dilution steps for the microbial abundance analysis

Dilution	Preparation
1:16	32µl no diluted sample (blank or sample) + 512 PBS
1:32	500µl 1:16 sample + 10µl SYBR green + 490µl PBS
1:64	500µl 1:32 sample + 10µl SYBR green + 490µl PBS
1:128	500µl 1:64 sample + 10µl SYBR green + 490µl PBS
- PBS is diluted to 10X (4ml PBS + 36ml deionized water) and filtered through 0.2 µm filter - SYBR green is diluted to 100X (2µl stock + 198µl PBS)	

The microbial counts were recorded, and the bacterial population was located based on the plots of green fluorescence channel (FL1) versus side scatter (SSC). The used settings are presented in table 2.

Table 2. Settings for the microbial count.

Parameter	Value
SSC gain	255
FL1 gain	450
Green fluorescence threshold (manually)	4000
Flow rate [µL/min]	10
Run time [s]	
Blank	90
Sample	120

Finally, the data analysis was achieved with CytExpert Acquisition and Analysis Software (Version 2.4.0.28, Beckman Coulter). The bacterial abundance average of the sample was calculated from the sample diluted by 1:32, 1:64 and 1:128. The results were plotted against the temperature and a t-test on the significance of the slope was performed.

4.5 Quantification of nitrate removal

To compare the bioreactor efficiency prior and after the installation of a heating device, two NO_3^- quantification methods have been utilized: NO_3^- removal efficiency over time and NO_3^- removal rate against temperature.

4.5.1 Nitrate removal efficiency over time

Nitrate removal efficiency (expressed as % of concentration at inlet) was calculated from the weekly analysis done by LKAB laboratory for three consecutive years (2020, 2021 and 2022). This method does not consider flow rate and is defined with the following equation (equation 5).

$$NO_3^- \text{removal } \% = \frac{([NO_3^-]_{in} - [NO_3^-]_{out})}{[NO_3^-]_{in}} \times 100 \qquad (5)$$

Where $[NO_3^-]_{in}$ corresponds to the NO_3^- concentration at the inlet and $[NO_3^-]_{out}$ is the NO_3^- concentration at the outlet.

4.5.2 Nitrate removal rate against temperature

Nitrate removal rate is defined as the NO_3^- depletion over time. The past and present measured NO_3^- concentrations from the different sampling profiles (inlet, outlet, and A/B-wells) and the weekly analysis done by LKAB laboratory were used to calculate the NO_3^- removal rates. Each consecutive point was assumed to be part of a theoretical flow path along the bioreactor which represented NO_3^- concentration changes over time. Two approaches were used to estimate NO_3^- removal rates: by calculation and by graphical interpretation. The results were then plotted against temperature and a model was fitted to the data by regression.

The calculation of NO_3^- removal rate uses the difference in NO_3^- concentration, obtained from LKAB weekly analysis, between the inlet and the outlet and multiplied it by the flow rate (equation 6).

$$NO_3^- \text{removal rate} = ([NO_3^-]_{in} - [NO_3^-]_{out}) \times Q \qquad (6)$$

Where $[NO_3^-]_{in}$ corresponds to the NO_3^- concentration at the inlet, $[NO_3^-]_{out}$ the NO_3^- concentration at the outlet and Q the average daily flow rate. Both concentrations are in [mg L^{-1}] while Q is expressed in L s^{-1}. The results are thus given in mg s^{-1}. However, this should be noted as a rough estimation.

The graphical interpretation of NO_3^- removal rate is based on nth order rate law. The NO_3^- concentrations for three different sampling profile periods (2019, 2020 and 2022) were plotted against cumulative time. Velocity is an important parameter used to estimate the cumulative time. To determine its value for any given flow rate, a calibration curve was constructed between these two variables. Velocity was calculated from the available conductivity values of the inlet and the outlet from 2019 to

2022. By observing the response delay in a conductivity peak from the inlet to the outlet and knowing the distance between these two points, it was possible to determine velocity with the following simple equation (7).

$$v = \frac{d}{t} \qquad (7)$$

Where v refers to the velocity (in md^{-1}), d to the distance (in m) and t to time (in d). The resulting velocities were then plotted against their respective flow (average flow of the delay period) and a calibration curve was created (appendix E). The results from a tracer test performed in 2020 (Herbert 2020a) were also added as input for the calibration curve. The cumulative time, used for determining the NO_3^-removal rate, was determined using the corresponding velocity given for the actual flow rate and the distance between each consecutive point as defined in the following equation (7). Finally, the NO_3^-concentrations in the bioreactor are plotted as a function of cumulative transport time, and a linear model was fitted to the data. Plotted as concentration vs time and as ln concentration vs time. The highest coefficient of determination R^2 defined if the 0^{th} or 1^{st} order rate law represented the best fit for the results. The slope value is equal to the removal rate result which is given in mg L^{-1} h^{-1}. This method is more accurate than the numerical method but requires some personal interpretation which could induce errors.

The results are represented as “grouped approach” and “individual approach” for each year. The grouped approach considered all profile sampling within a period while the individual approach considered the difference in temperature between each sampling profile for 2019 and 2020 and within each profile for 2022 where rates were generally estimated from positions along the profile where there was constant temperature between one point to another (appendix E).

4.6 Energy consumption

To assess the economic aspect of this experiment, an energy logger (Dranetz PX5, Beving, Farsta, Sweden) had been installed near the heater from the 12^{th} to the 16^{th} of May to measure its cumulative energy consumption in kWh. Since cumulative values were provided from the device, hourly averages were extracted and subtracted from one another to obtain the actual energy consumption per hour. The final price for the cold season was then calculated by multiplying this value with the LKAB kWh prices (0.35 SEK kWh^{-1}, LKAB, pers. comm.). The difference in temperature before and after the water goes through the heater was also considered.

5 Results

5.1 Flow rate

As mentioned in the previous section, the flow was turned off during the winter period and officially started again on the 10th of January. Even though some fluctuations could be observed over the study period (figure 5), the flow was considered rather constant with an average of 0.10 L s^{-1}.

In fact, the flow was turned off from the 18th to the 23rd of February for maintenance purpose. Additionally, the sensor encountered some issues and flow rate values were underestimated compared to the actual value of 0.10 L s^{-1} given by the manual measurements (figure 5). Both of which had an overall underestimating impact on flow rate values. Therefore, low values were not considered for further analysis and replaced by 0.10 L s^{-1}. Moreover, according to the calibration curve between flow rate and velocity (appendix E), it would represent a velocity of 1.5 m d^{-1}. Thus, the theoretical hydraulic residence time for the DBR was 25 days.

Two major flow peaks could be observed at the beginning (3rd of February) and at the end of the study period (26th April). The first one was deliberately provoked and reached up to 0.15 L s^{-1} before being decreased back to 0.11 L s^{-1} on the 7th of February. However, the second one could be an indication of the beginning of the snowmelt period.

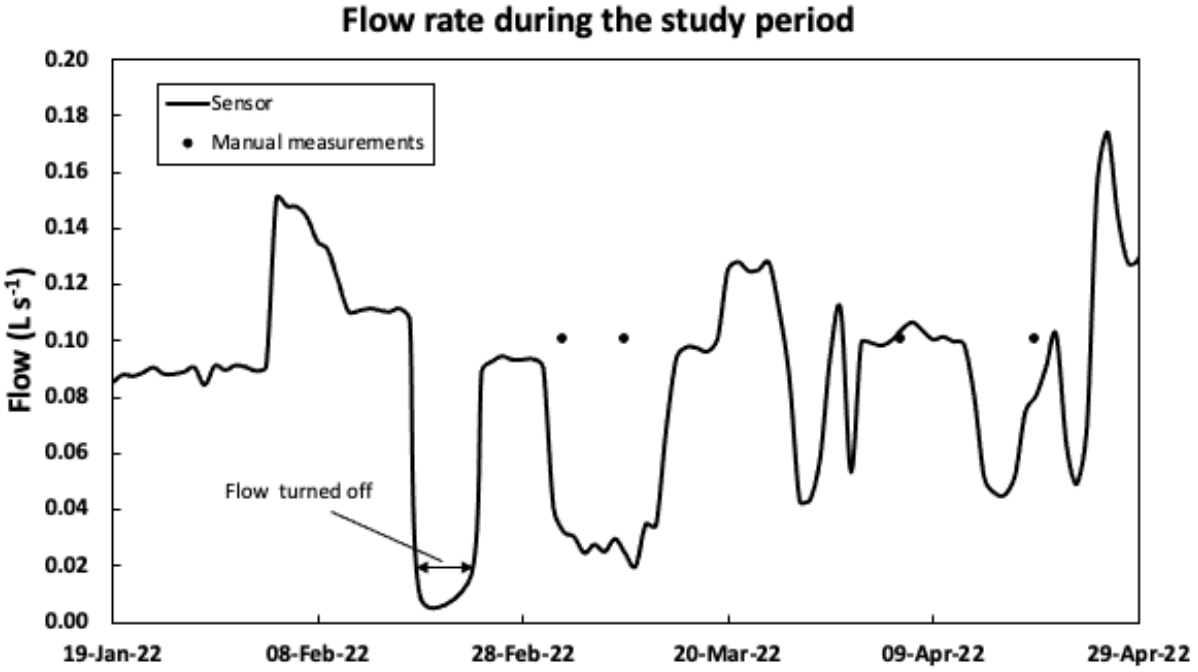

Figure 5. Flow daily averages along the study period.

5.2 Temperature

Beginning with the starting point of our experiment on the 20th of January 2022 (line 1, figure 6) heating was not constant due to the heater breaking down twice. This occurred first on the 18th of February, finally getting repaired on the 4th of April, and then again on the 22nd of April (line 2, 3 and 4, figure 6).

The heaters warmed the water up to 20°C during this first interval and 30°C during the second (figure 6.a). A peak of over 20°C could be observed on the 12th of March probably due to a momentary heat surge during repairs but did not have any major consequences on the DRB temperatures. No major heat losses were observed between the heater outlet (heater out) and the DBR inlet (Tinlet).

In contrast, as seen in figure 6.b, the highest temperatures within the bioreactor do not exceed 11°C. The sensors are placed along a line even though the mobile sensors were installed slightly deeper than the permanent sensors (figure 3.b). In figure 6.b, the sensors located furthest from the inlet (from T1B to T5B) showed a greater response delay and a lower temperature rise after each heater start (line 1 and 4, figure 6.b). T5B, being the last measured point, barely shows any increase. However, it appears that the mobile sensor T1B (deeper) temperature maxima is lower than T1 even though the distance from the inlet is shorter.

The reverse effect is also perceived. After the heater broke down the first time (line 2, figure 6.b), the decrease in temperature exhibits a delay with distance as T1B is the first one to decline followed by T1, T2, T3 and T4. The temperature drop to initial values took up to 8 days for T1B, 10 days for T1 and 25 days for T2 while T3 and T4 did not go down to their original values. Furthermore, the declining slopes are lower for T2 and T3 than T1B and T1.

(a)

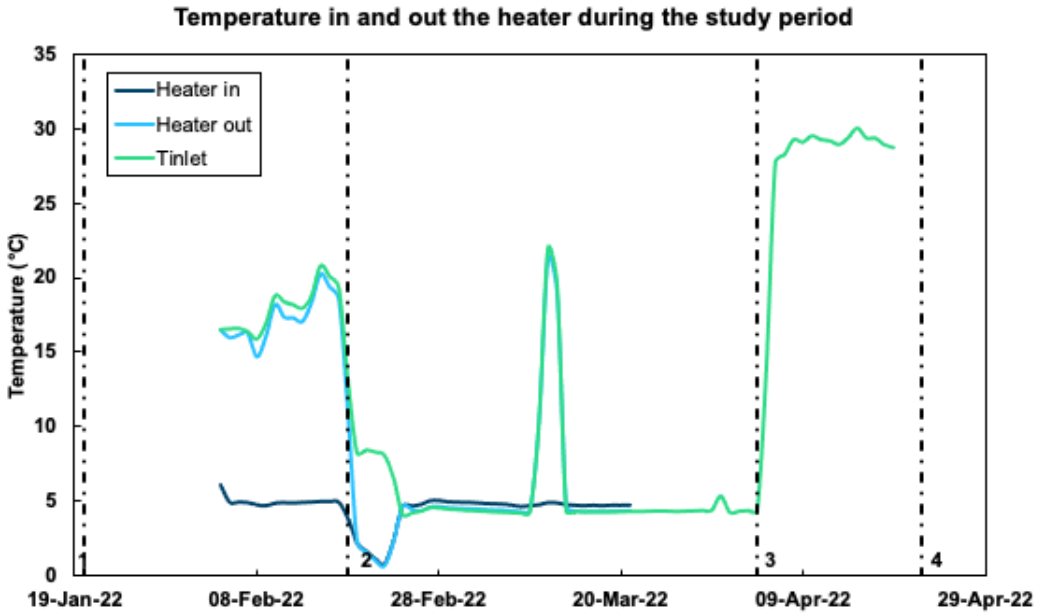

(b)

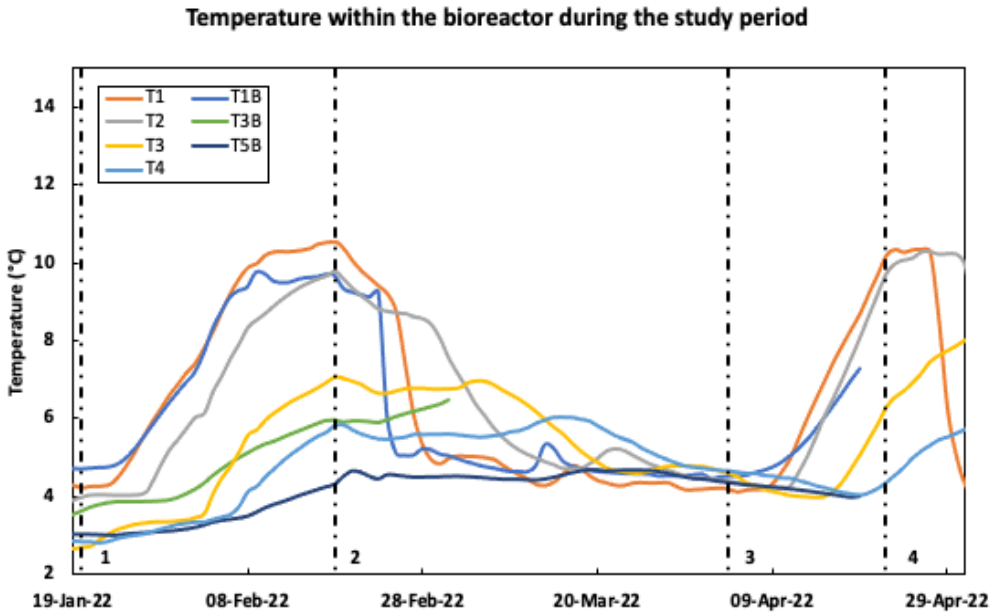

Figure 6. Evolution of the temperature during the study period. Lines 1 and 3 represent the time when the heater was started while 2 and 4 are the time when the heating stopped due to heater failure.

a. Measured water temperature going in (heater in) and out (heater out) of the heater and at the inlet (Tinlet).
b. Measured water temperature at the different sensors (permanent sensors (shallower): T1,T2,T3,T4 and mobile sensors (deeper): T1B, T3B, T5B).

The temperature profiles in figure 7 display three different heating episodes in the bioreactor. The 29th of March, representing the pre-heating period, has a temperature average of 4.5°C and does not present any variability neither with distance nor depth.

Contrary to this, the 12th (heating period) and the 26th of April (post-heating period) have an heterogenous temperature distribution with values reaching up to 27°C and 18°C, respectively. The highest temperatures are located closest to the inlet (within the first 15 m distance) and the shallow parts of the bioreactor. On the 26th of April, even though cold water enters at the inlet (0 m distance), warm temperatures proceeds further than on the 12th of April mainly in the shallower area.

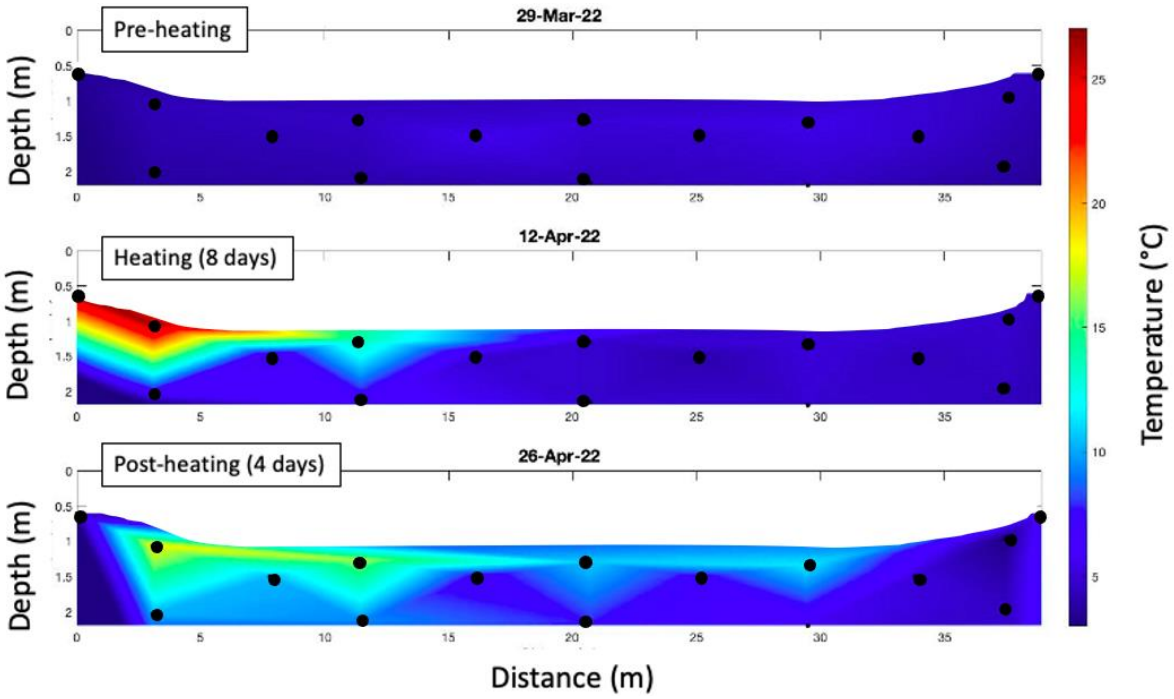

Figure 7. Temperature distribution within the bioreactor for different profile data. The black dots represent the measurements' location points (manual measurements and sensors).

5.3 Chemical analyses

The detailed results of chemical analyses can be found in appendix C.

5.3.1 Nitrogen compounds and temperature

A-wells (shallower) were sampled later than B-wells (deeper). On the 18th of February and the 3rd of March, all the shallow wells could not be sampled as the water in them was frozen (P3A-P4A-P5A for the 18th of March and P5A for the 3rd of April).

Nitrate concentration underwent a lot of variations but overall decreased with distance. The 19th of January and 3rd of March (Figure 8.a and d) display the same pattern with high NO_3^- concentrations, up to 135 mg L^{-1} N and 90 mg L^{-1} N, respectively, at the inlet (0m) and low values close to the detection limit after 20m. The temperatures are under 5°C for the 19th of January and 7°C for the 3rd of March. For the 12th and 26th of April, NO_3^- concentrations are at their lowest in A-wells compared to B-wells and the temperatures are higher in A-wells than B-wells (figure 8.g and h). The 8th of February, 21st of March and 29th of March (Figure 8.b, e and f) show a NO_3^- increase when it reaches the second well

(11.44m). This trend is seen in B-wells for the 8th of February and A-wells for the others. Finally, values in well P5B are generally close to the detection limits showing a NO_3^- depletion from P4B to P5B and a rise in the outlet again.

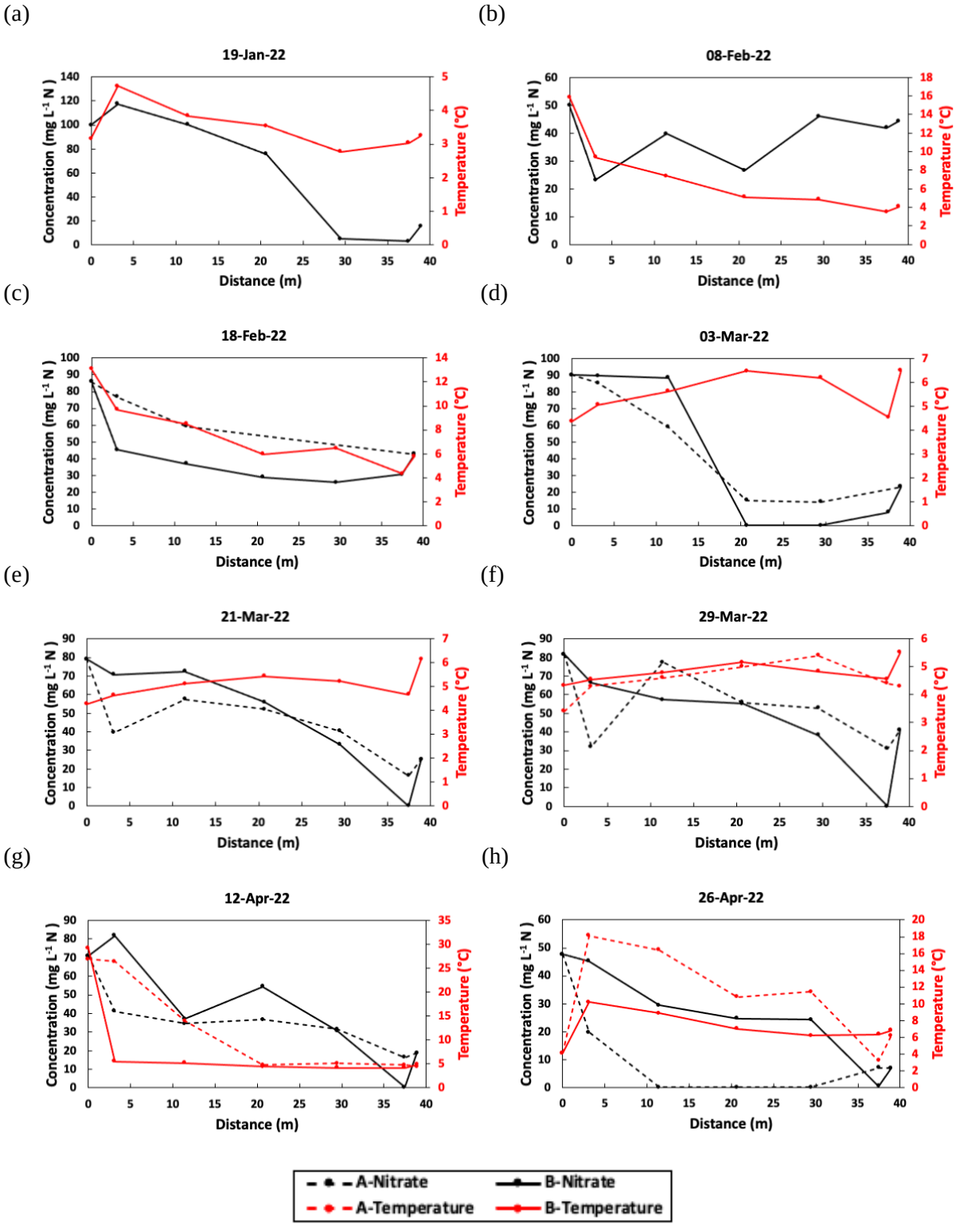

Figure 8. Nitrate concentrations obtained from the different sampling profiles. Under detection limit values are represented on the graph as y = 0.0075 mg L^{-1} N.

Nitrite peak concentrations ranged from 0.30 (figure 9.a) to 10 mg L^{-1} N (figure 9.d, B-wells). Similarly to NO_3^- concentrations, NO_2^- has gone through quite a lot of variation. The highest concentrations are mainly observed in the second part of the bioreactor, after 25 meters (P4 and P5) where the water is at its coldest (figure 9). Furthermore, except for the well P5, the shallow sections (A-wells) of the bioreactor, which are generally also warmer, have lower NO_2^- concentration than the deeper sections (B-wells).

Finally, NH_4^+ has low values not exceeding 1.5 mg L^{-1} N and indicating no major difference between the two depths except for the 26th of April (figure 9.h). It has, however, shown a slight increase with temperature as seen in figure 9.g and 9.h where higher concentrations are observed in A-wells, warmer than B-wells.

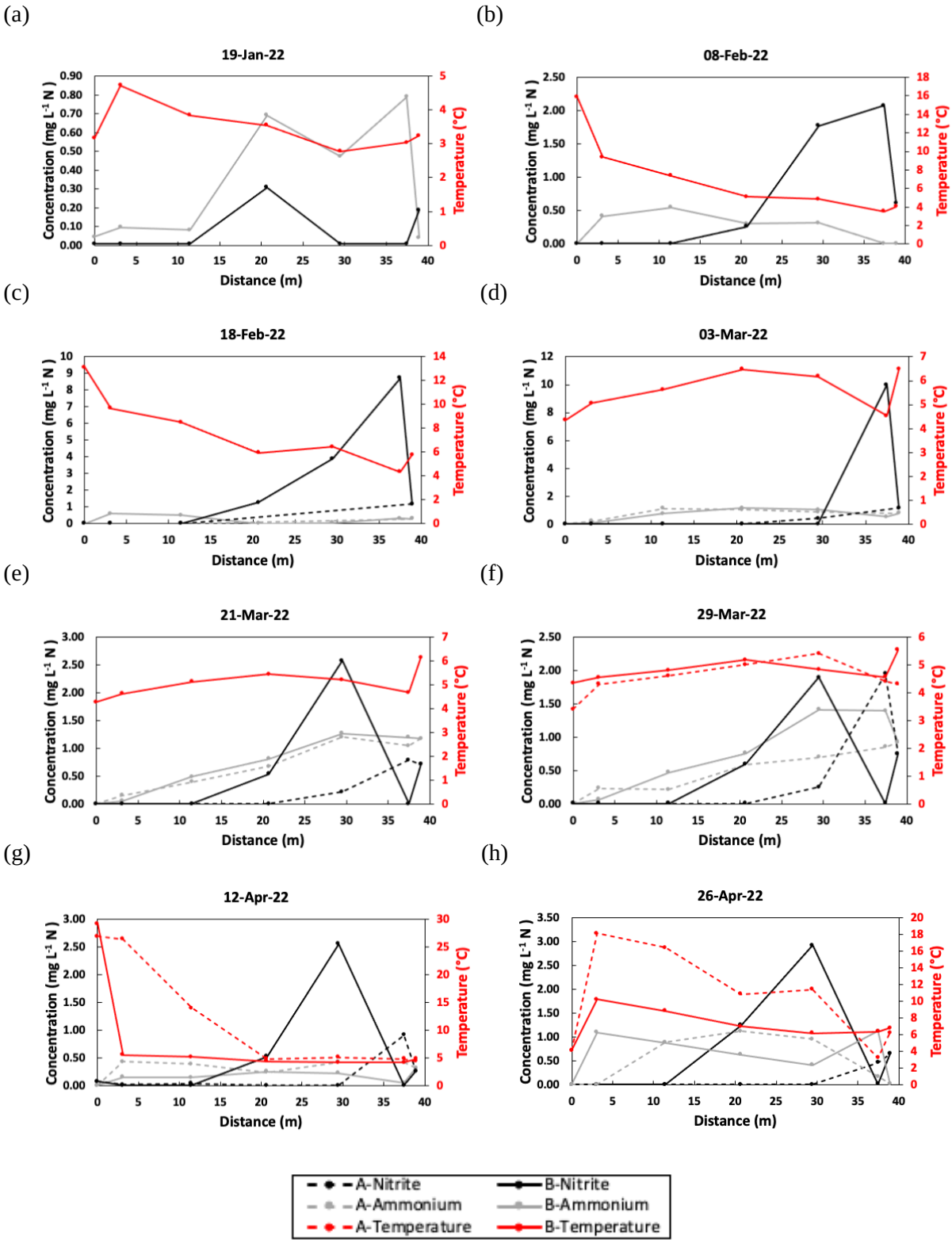

Figure 9. Nitrite and ammonium concentrations obtained from the different sampling profiles. Under detection limit values are represented on the graph as y = 0.0075 mg L^{-1} N.

5.3.2 Total phosphorus, dissolved phosphorus, and total organic carbon

5.3.2.1 PO_4-P

PO_4-P concentrations are low and do not exceed 15 µg L^{-1} P (P4B on the 29th of March, table 3). It appears however that, within the bioreactor (form P1B to P5B) the values are lower in the first section (P1B to P3B) for the 21st and 29th of March while the reverse is observed for the 12th and 26th of April.

Table 3. PO4-P values at different time and position.

Date	Inlet (µg L^{-1} P)	P1B (µg L^{-1} P)	P2B (µg L^{-1} P)	P3B (µg L^{-1} P)	P4B (µg L^{-1} P)	P5B (µg L^{-1} P)	Outlet (µg L^{-1} P)
21-Mar-22	<1	<1	<1	4	12	<1	6
29-Mar-22	<1	<1	2	2	15	2	5
12-Apr-22	<1	<1	3	<1	1	<1	2
26-Apr-22	<1	7	5	4	2	1	<1

5.3.2.2 Relationship between TOC, tot-P and temperature

According to figure 10, TOC and tot-P increase with temperature. Moreover, the correlation coefficient between TOC and Tot-P including P5B is equal to 0.57 while it is 0.65 by excluding P5B. While excluding P5B, R^2 values are also higher, from 38.1% to 80.5% for TOC and from 17.7% to 27.1%.

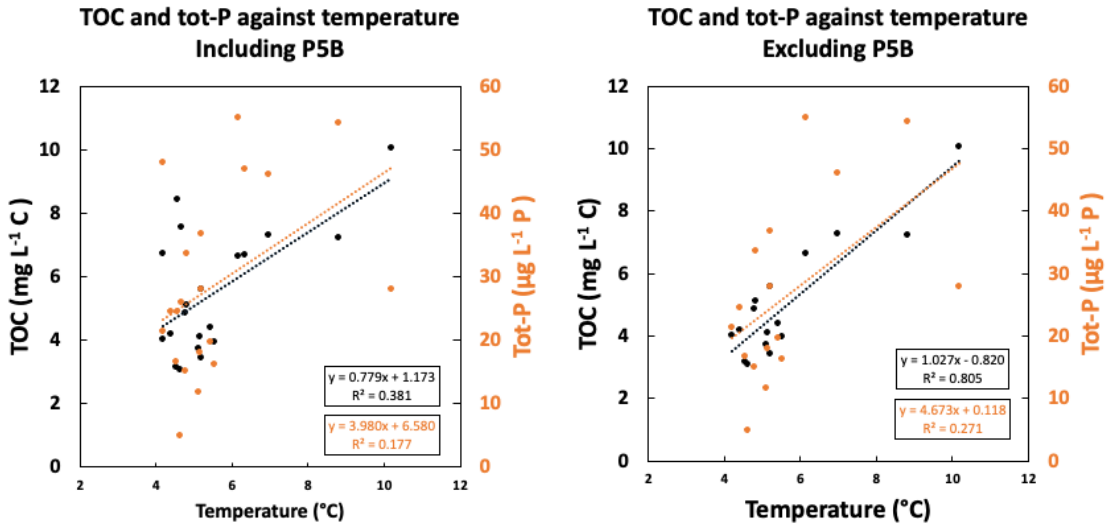

Figure 10. TOC and tot-P against temperature including P5B (left) and excluding P5B (right).

5.3.2.3 TOC/NO_3^- ratio

The TOC/NO_3^- ratio fluctuates under 0.35 for all points except 5PB, which is extreme and reaches up to 1122 (figure 11). This ratio does not vary and shows a rather straight line until a more noticeable increase of approximately 0.15 from the 12th to the 26th of April.

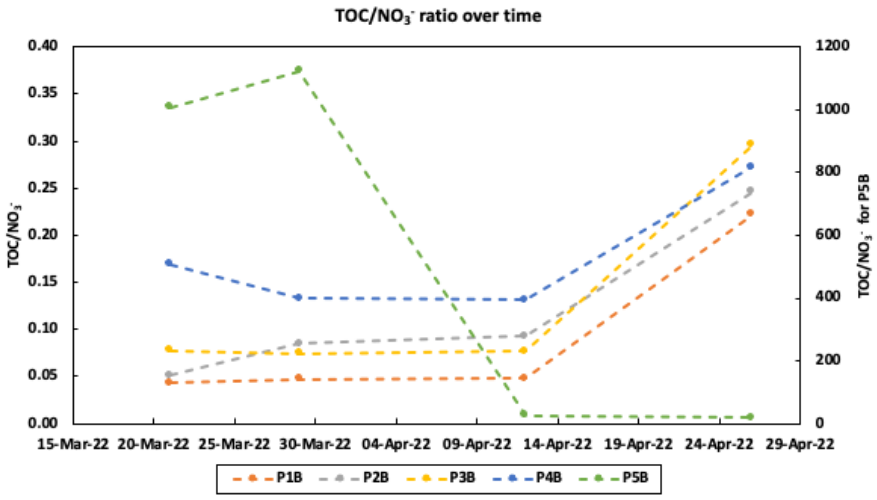

Figure 11. TOC/NO_3^- ratio against time. P5B is plotted on the secondary y-axis.

5.3.3 Sulfate

Snowmelt can have a diluting effect on the bioreactor waters and thus biases the chemical analysis interpretation. Therefore, SO_4^{2-} analysis was needed for the 26th of April as flow rate indicated high values that could be linked to the start of the snowmelt period (see figure 5). The high concentrations value measured in all the shallow wells, except for the last one which is under detection limit, indicate that no major snowmelt effect is present along the DBR profile (table 4).

Table 4. Sulfate result of the A-wells sampling profile 26th of April 2022.

Well	Concentration (mg L^{-1})
P1A	527.4
P2A	601.2
P3A	518.5
P4A	650.4
P5A	< 40

5.4 Bacterial abundance

The microbial abundance stayed within the same order of magnitudes from 10^6 to 10^7 event mL^{-1} for all the profile samplings (figure 12). The relationship between abundance and temperature is not clearly observed for the entirety of the bioreactor. However, the result of the t-test, showing p-values under 5%, indicated that the positive relationship between bacterial abundance and temperature is significant for the first section of the bioreactor (P1B to P3B) with R^2 higher than 73% (figure 12 and table 5). In contrast, no significance was observed for the second section with R^2 being under 16% for P4B and 2% for P5B (table 5).

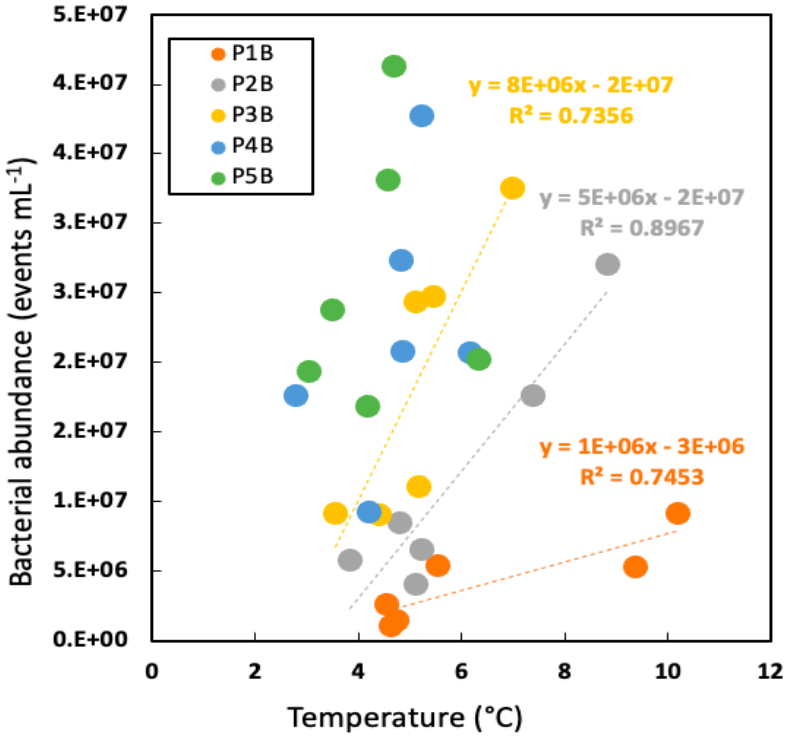

Figure 12. Bacterial abundance in events (=count) mL^{-1} against temperature. R^2 and linear regression equation are only displayed for significant slopes determined by the t-test in table 5. The results from the 18th of February and the 3rd of March are not shown since the analysis conditions were not optimal for those two dates and an important bacterial loss occurred. However, a summary table which contains all the results can be found in appendix D.

Table 5. Statistical analysis on the linear model slope, t-test. The null-hypothesis is H0: b=0.

Wells	t-test (p-value)	R^2
ALL	0.924	$3*10^{-4}$
P1B	0.027	74.5
P2B	0.004	89.7
P3B	0.029	73,6
P4B	0.439	15..6
P5B	0.803	1.7

5.5 Quantification of nitrate removal

5.5.1 Nitrate removal efficiency over time

Between 2020 and 2021, the time at which not heating device was installed, a decrease by almost half in the mean NO_3^- removal was observed (figure 13). The removal progressed from 61% to 32% considering the full period and from 43% to 28% only considering January to May.

In contrast, the highest mean NO_3^- removal mean with a value of 65% was observed during the study period in 2022, the year of the installation of the heating device. This value has more than doubled compared with the same period in 2021. Two major peaks increase to 97% on the 27th of January and the 10th of March 2022 can be seen. Furthermore, NO_3^- removal reached a plateau around 55% twice:

from the 10th to 17th of February and from the 24th of March to the 3rd of April. Even though these results are similar, these two periods, however, define two distinct events. The first period is linked to a warming period (the heater is on, after line 1, figure 13) while the second is related to a cold period (the heater is broken, after line 2, figure 13).

Finally, even if NO_3^- removal dropped at end of the period, it remained higher than the two previous annual values for the same period over 45%.

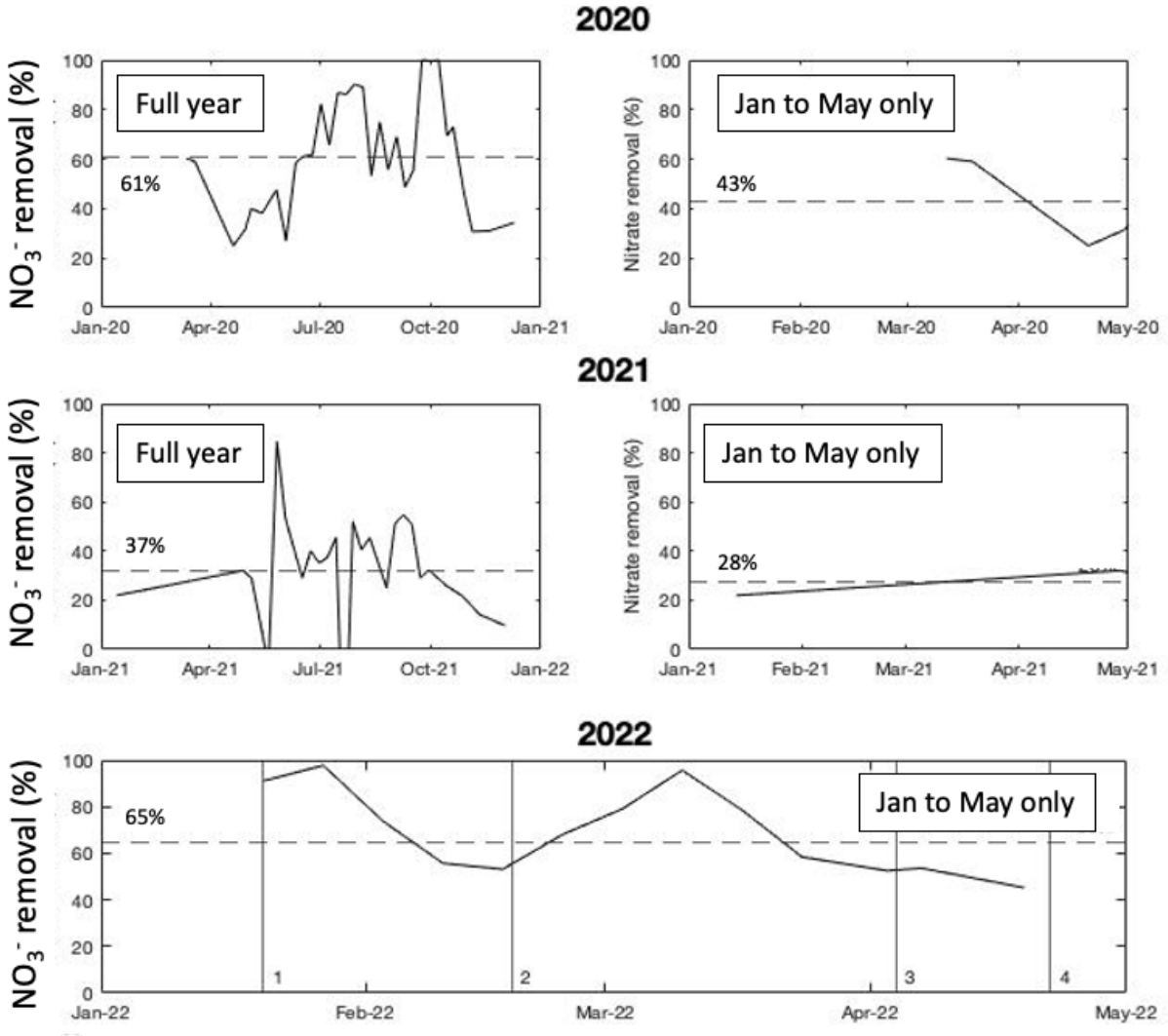

Figure 13. Nitrate removal (%) between three consecutive years in BR3. The dotted lines represent the average removal for the full represented period. Both 2020 and 2021 did not possess a heating system compared to 2022. For 2021, the full year mean NO_3^-removal was calculated by excluding values going under 0. For 2022, the values before the 3rd of February were not considered to calculate the average as old water was mixed within the system and thus not representative. Line 1 and 3 show when the heater starts while 2 and 4 show when heating stopped due to heating failure.

5.5.2 Nitrate removal rate and temperature

The NO_3^- removal rates, obtained by calculation with the NO_3^- concentrations from the inlet and the outlet, shows a positive relationship with temperature for 2020 and 2021 while displaying a negative relationship for 2022 (figure 14). The fitted lines between 2019 and 2020 shows a net decrease in removal rate at the same temperature while the ones from 2020 and 2021 shows similar rate for a range of temperatures. However, it is important to note that the R^2 values are all under 25%. Going from 23.19%, 13.92% to 6.31% for 2020,2021 and 2022, respectively. A t-test performed on the significance a linear model slope between log of NO_3^- removal rate and temperature gave p-values over 5% for 2020 and 2022 (7% for 2020 and 48% for 2022) and thus indicate no significance relationship between these two variables.

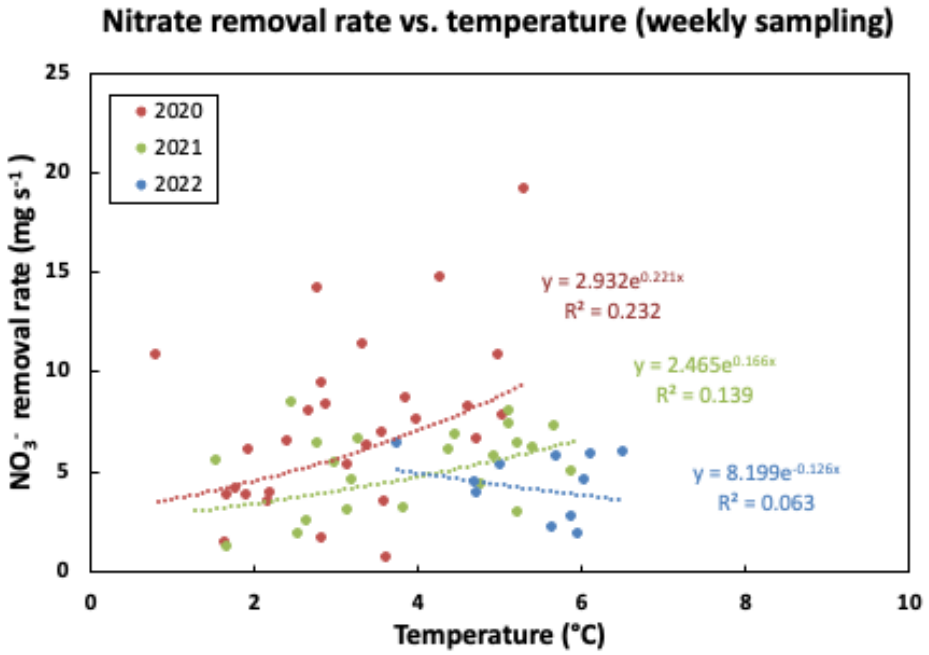

Figure 14. Nitrate removal rate against temperature done by calculation method for 2020, 2021 and 2022. The p-values were given by a t-test (null-hypothesis H_0: b=0) on the significance of a linear model slope between log10 of NO_3^- removal rate and temperature and are equal to 0.070, 0.039 and 0.483 for 2020, 2021 and 2022 respectively.

The NO_3^- removal rates, obtained by graphical interpretation, against temperature are presented in figure 15. The detailed steps of this method are presented in appendix E. For the 2019 sampling profiles, the 1st order rate law generally gave higher R^2 values and therefore was chosen to estimate NO_3^- removal rates. In contrast, both 2020 and 2022 sampling profiles received higher R^2 values for the 0th order rate law. The grouped approach represents only few data points. Thus, it will not be considered for interpretations (figure 15.a). The individual approach took into account temperature variations to obtain NO_3^- removal rates and more data points have been considered (higher resolution). The R^2 is 35.3% and the activation energy given by the model is equal to 17 $kJ.mol^{-1}$. However, a cluster can be observed at low temperature values.

(a)

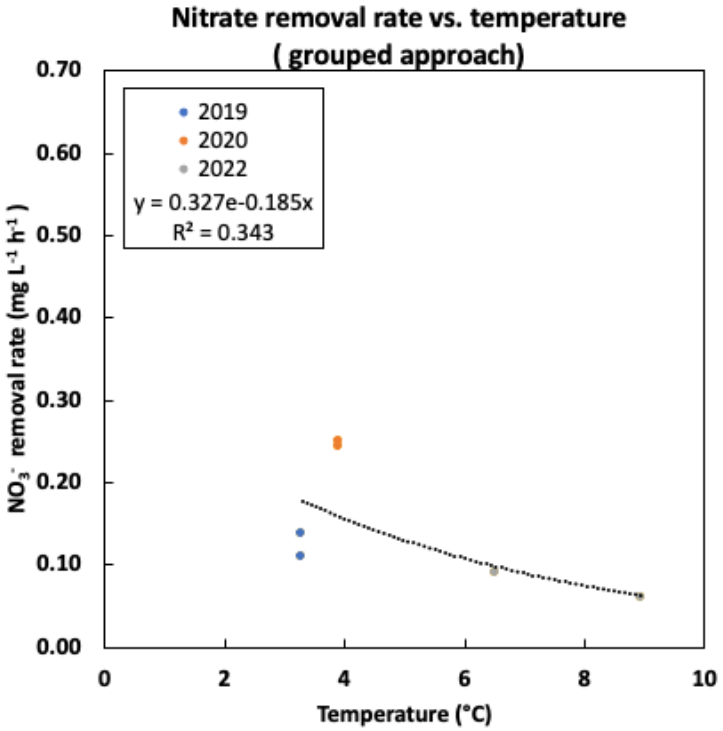

(b)

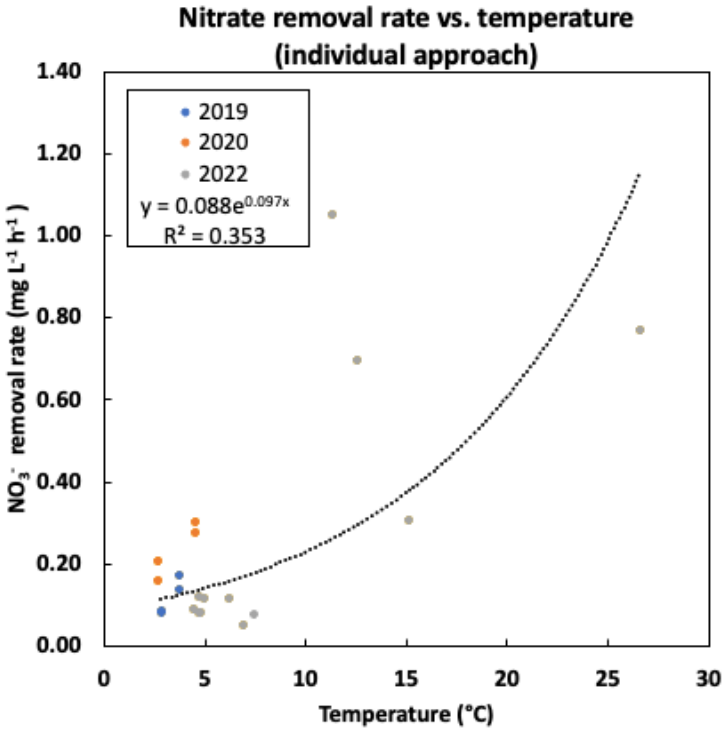

Figure 15. Nitrate removal rate against temperature done by graphical interpretation for 2019, 2020 and 2022.

a. Grouped approach which considered all profiles within a period to obtain NO_3^- removal rates. A lack of significance was observed.
b. Individual approach which considered temperature variations to obtain NO_3^- removal rates. The resulting activation energy (Ea) is equal to 17 kJ mol^{-1}.

5.6 Energy consumption

The energy consumption was observed to be rather stable with a value of 10.46 kWh between the 12th and the 16th of May and corresponded to a water temperature increase of approximately 24.12°C (figure 16). This led to water temperature going up to 35°C with an average of 30°C at the inlet.

The heater operational cost is 3.66 SEK h^{-1} which correspond to 15991 SEK for the full cold months period (table 6).

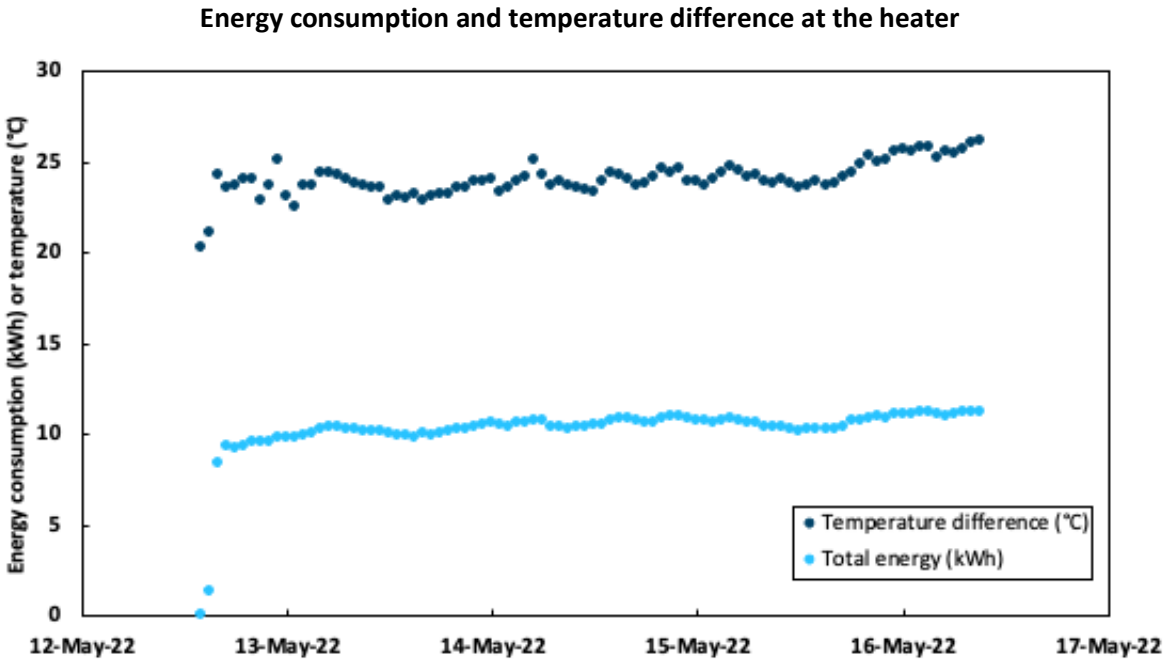

Figure 16. Energy consumption and temperature difference between the water coming in and out of the heater. The mean temperature difference is 24.12°C while the mean total energy is 10.46 kWh.

Table 6. Heating operational cost considering the LKAB price of 0.35 SEK kW h^{-1}.

	Energy consumption (kWh)	**Price (SEK)**
For 1 hour	10.46	3.66
For the cold months (October-March: 182 days)	45689	15991

6 Discussion

6.1 Bioreactor temperature and its relation to flow

During the study period, while the heater was working properly, the temperature was observed to decrease along the distance from the heating source and with depth in the bioreactor (figure 6 and 7). An important heat loss was detected between the inlet which reached up to 30°C and the first sensors where the temperature barely reached 11°C (figure 6). Heat loss is driven by temperature differences. As the warm water enters and comes in contact with the cold bioreactor water and substrate, part of the heat will be transferred by conduction, especially along the sides and the bottom of the bioreactor. This phenomenon is observed along the bioreactor as temperature maxima of the inflowing water decreases with distance from the DBR inlet. Moreover, the delay in temperature response detected by the sensors is linked to the movement of the incoming water which is the main heat transfer process in the system. Even though these observations were mostly made for the deeper sections of the bioreactor, since most of the temperature sensors were located in deeper regions, a similar effect was also occurring in the shallow regions. In fact, at the beginning of this experiment, the shallower A-wells, were frozen in the second half of the bioreactor. This could be explained by the influence of the air temperature, which dropped below -20°C during this period, for example if there was defective insulation. This effect could not be balanced as heating was still in its early stages and did not have the time to cover the entirety of the DBR.

The temperature within the DBR decreased with depth, indicating that much of the warm water propagated further across the shallow parts of the bioreactor (figure 7). A hypothesis could be that the flow rate is unevenly distributed along the DBR and has a greater velocity closer to the surface (appendix F). This phenomenon could be observed during the first heating period where the temperature maximum at the deeper T1B sensor was lower than the temperature maximum at the shallower T1 sensor, even though T1 was placed closer to the inlet (figure 6.b). This suggests that the inflowing warm water primarily comes in contact with the shallow sensors while avoiding the deeper ones and therefore temperature rise more slowly in the deeper sections. Moreover, the A-wells were observed to generally be warmer than the B-wells (figure 7, 8 and 9).

During the study period, higher temperature water could not properly propagate across the entire bioreactor due to the heater breaking down twice. Therefore, it was not possible to reach a steady state with a constant temperature gradient and the temperature spread was unevenly distributed across both the distance and the depth. When the heater malfunctioned, cold flowed into the bioreactor, and similar to the heating period, the cold front can be observed to propagate through the DBR. This was linked to the inflow velocity which mainly propagates heat along the system. Furthermore, it was difficult to maintain steady due to technical problems, with no flow from the 18th to the 23rd of February (figure 5). During this period, temperature depletion was rather constant for the first sensors (T1B and T1) as heat transfer mainly occurred through conduction. When the flow started again, an important temperature

drop of almost 5°C has been observed (figure 6.b) as cold water was pumped to the system and pushed the original warm water to the outlet. This can be observed in figure 7 and 8.d,e,f where warmer temperatures extend into the second part of the bioreactor.

During snowmelt, water flows vertically into the bioreactor since there is no impermeable cover, resulting in an increase in flow. A flow rate peak was observed in late April and could represent the start of the snowmelt (figure 5). This increase of flow could dilute the waters and lead to misinterpretation of the chemical analyses during this period. However, since SO_4^{2-} concentrations were high all along the shallow parts of the bioreactor, the hypothesis of meltwater having a significant impact on the chemistry of our last sampling profile has been rejected.

6.2 Flow near P5

The observed concentrations in well P5A (especially NO_3^- and SO_4^{2-}) seem abnormal as P5 was assumed to lie along the theoretical flowpath of the bioreactor. However, P5 (A and B) presented unexpected concentrations results for almost all the performed chemical analyses. A drop in concentrations under the detection limits for NO_3^- and NO_2^- was observed at the end section of the bioreactor, primarily in well P5 (A and B) (figure 8 and 9). Similarly, figure 10.b indicates that the correlation between TOC and tot-P versus temperature gave better results when excluding P5B and the TOC/NO_3^- ratio showed extreme values for this well (figure 11). This might imply that the flow is not uniform within the system along the entire distance and passes to the side of P5 to directly join the outlet at the side of the bioreactor (appendix F). A similar observation was noted during the tracer test performed in 2020 where low concentrations of bromide (Br used as tracer) were lower than expected from P3 to P5. This is assumed to result in a much narrower plume of flow that did not cover the entire width of the bioreactor (Herbert 2022). Therefore, P5 has been considered as an outlier for our interpretations.

6.3 Denitrification efficiency

Nitrate concentrations in the inlet fluctuated during the study period. However, the overall concentrations decreased with distance highlighting the denitrification process within the bioreactor (figure 8). On the 12th and 26th of April, NO_3^- concentrations were lower in the shallow areas which showed warmer conditions (figure 8.g and h). This could suggest that an increase in temperature leads to a greater NO_3^- depletion.

Prior to the heater installation (between 2020 and 2021), a decrease in the overall bioreactor efficiency, defined in this case by the mean NO_3^- removal, had been observed (figure 13). This phenomenon could be linked to bioreactor substrate aging, inducing a loss in carbon availability which in turn reduces denitrification efficiency as seen in previous studies (Schipper et al. 2010; Ghane et al. 2015; Nordström & Herbert 2019). However, during the study period, this efficiency almost doubled to a value of 65% compared to the previous year (figure 13). Furthermore, this increase is greater when

compared to the same time interval during 2021 (from January to May). Therefore, considering that all years experienced the same environmental conditions with the exception of temperature, it appears that the heater has been proven effective in improving the NO_3^- removal efficiency. Moreover, two plateaus were attained at 45% NO_3^- removal during both warm and cold periods (figure 13). This could imply that heating up the water continuously is not necessary to achieve better denitrification results and that boosting the system by heat-pulse could be enough. However, this method would require further investigations as denitrification can be affected by numerous factors (see section 3.2).

Nitrate removal rates have generally increased with temperature (figure 14 and 15). However, the low R^2 indicates that the observed outcomes are not well represented by these models and no strong conclusions could be extracted from the regression analysis. The calculated NO_3^- removal rates from the weekly sampling of the inlet and the outlet indicated decreasing rates from 2020 to 2021 (figure 14), which agrees with the observations made previously where the denitrification efficiency decreased with time when the system is not provided with a heating device. Moreover, even though no strong significance was observed for 2020, the log of NO_3^- removal rate showed a positive relationship with temperature for 2021. In contrast, 2022, which has a R^2 lower than 7%, displays the lowest NO_3^- removal rates with a negative relationship between rate and temperature. Moreover, the relationship between the log of NO_3^- removal rate and temperature was proven not significance with a p-value being over 45%. The main uncertainties linked to this method are that flow rate has been changing through time and that the taken temperatures and concentrations do not consider the internal variations in the bioreactor. Although 2020 and 2021 did not experience any major temperature changes from the inlet to the outlet, 2022 showed large differences of temperature along both the distance and the depth (see section 6.1). Therefore, an underestimation of rate linked ot higher temperatures is likely to occur. Furthermore, it is important to remember that the bioreactor has a hydraulic residence time of 25 days, and the concentrations present in the outlet do not correspond to the same event in the inlet.

The NO_3^- removal rates that were estimated graphically by the individual approach (figure 15.b) gave a slightly better estimation with a R^2 of approximately 35%. Indeed, it is more accurate as more data points and temperature variations have been considered. The best fit for the rate law switched from a 1^{st} to a 0^{th} order reaction from 2019 to 2020 (appendix E) which agrees with previous studies which indicated that such changes would occurs as the bioreactor ages (Ghane et al. 2015; Nordström & Herbert 2019). A positive relationship between denitrification rate and temperature has been highlighted and seems to be in agreement with the Arrhenius equation defining rate as a positive exponential relationship with temperature (Schipper et al. 2014; Arcus et al. 2016). The resulting activation energy (Ea) of 17 kJ mol^{-1} is small compared to values presented for denitrification by Takenaka et al. (2011) but agree rather with the value of 23.55 kJ mol^{-1} obtained by Nördstrom (2014) utilizing the same method when not considering rates limited by low NO_3^- concentrations (0^{th} order rate law). The (Ea) value was obtained with the optimized parameters given by the model using equation 3. Since the heating system broke twice, a constant temperature gradient was not reached and removal rates for

higher temperatures were not sufficient to either estimate an optimal temperature or improve the removal rate-temperature model.

6.4 By-products

Other nitrogen compounds have been detected in the bioreactor. Nitrite can be considered a key indicator of incomplete denitrification (see equation 2, Nordström & Herbert 2018). Nitrite concentrations were lower in A-wells (shallower) than B-wells (deeper) and overall increased with distance along the DBR (figure 9). These differences could be linked to the temperature distribution within the bioreactor (see section 6.1) where higher temperature leads to lower NO_2^- concentrations which therefore boosts complete denitrification.

Ammonium concentrations where under the range of 1.5 mg L^{-1} N and showed no major difference between the two depths except for the 26th of April where higher concentrations are generally observed for the shallower, warmer sections of the DBR (figure 9.h). Therefore, even if DNRA also seems to have been affected by temperature changes, denitrification has been identified as the main process occurring within the bioreactor. This agrees with other studies which suggests that denitrification is the main process occurring within the bioreactor (Warneke et al. 2011; Nordström & Herbert 2018; Nordström et al. 2021).

6.5 Other parameters potentially impacting denitrification

Even though temperature is an important factor, other processes could impact denitrification efficiency (see section 3.2). Total phosphorus (tot-P) and total organic carbon (TOC) concentrations were shown to increase with temperature (figure 10). Furthermore, their high positive correlation to each other indicate a similar origin. Additionally, dissolved phosphorus (PO_4-P) was higher in the first section of the bioreactor relative to the further section the 21st and 29th of March, but the situation was reversed on the 12th and 26th of April (table 3). These two periods respectively correspond to the cold period and the warm period. Therefore, it could suggest that higher temperature would induce an increase in both tot-P, PO4-P and TOC. Hydrolysis could be one of the processes leading to the production of P and TOC from the woodchips which are used as a nutrient and energy source, respectively, by bacteria and enhance denitrification (Hunter 2003; Ng & Kim 2007; Ghane et al. 2015; Nordström & Herbert 2019). These results agrees with previous findings defining hydrolysis a temperature dependent process (Sun & Cheng 2002).

There appears to be a relationship between bacterial abundance and temperature in the bioreactor, but the relationship is not clear when considering all the sampling points in the DBR. However, a t-test revealed the positive correlation between bacterial abundance and temperature for the first three wells (from P1B to P3B) to be significant (table 5). No such conclusion was confirmed for the end section of the bioreactor. This could be related to the small temperature variations occurring in those wells which

were insufficient to present significant results or potential trends. The relationship between bacterial abundance and temperature has, thus, generally agreed with past studies defining temperature as a parameter that promotes microbial growth (Schipper et al. 2010; Maxwell et al. 2020).

6.6 Financial overview

The hourly energy consumption is equal to 10.46 kWh and represents a total cost of 15991 SEK for the cold months (table 6). This value is linked to a 24.12°C increase (figure 16) for a resulting water temperature at the inlet of ~30°C. This level of heating is rather excessive, and it is possible to heat to a less degree. Furthermore, it was shown that NO_3^- removal up to 45% could be reached even if the heater was turned off as seen with the plateau reached in figure 13. Considering the possibility of a long-lasting effect of heating on denitrification and the slow drop in temperature, water could be warmed up via a "heat pulse". This, in addition to the fact that the heater would not likely be operated for the entire winter period and would stop as soon as the effect of snowmelt is observed, would reduce the estimated operational cost.

6.7 Limitations and suggestions for further investigations

During this study, some uncertainties arose and would requires further investigations. First, a preferential flow seems to be present in the shallow parts of the bioreactor. A possibility is that the woodchips might be more compacted in the deeper parts and therefore have a lower hydraulic conductivity. Moreover, the main flowpath is uncertain and seems to avoid P5 to instead flow directly toward the outlet (appendix F). As a result, heat was not evenly distributed and the bioreactor efficiency could be lower than expected as studies have shown that pores that are not included in the main flowpath have low to inexistant denitrification reactions (Cameron & Schipper 2010). Therefore, by ensuring a more distributed flow through the bioreactor, its full volumetric capacity of the bioreactor could be used. One solution would be to locate the outlet along the desired flowpath instead of being placed on the side.

Another suggestion would be to reach a constant temperature gradient and then sampling the water chemistry, thus avoiding difficulties with data interpretation caused by the mixing water phenomemon in the bioreactor. Furthermore, differences in depth and distance of temperature measurement devices also induced errors in temperature estimation for the profile sampling. In order to have better understanding of the heating propagation and NO_3^- removal rates within the bioreactor, more temperature and NO_3^- measurements devices could be installed at known depths and distances. A 2D/3D model could be used to investigate temperature depth variations as the established temperature profile assumes flow along one flowpath which is not representative of realistic conditions.

7 Conclusion

This study has shown that heating the water prior to treatment within a bioreactor leads to enhanced NO_3^- removal. Indeed, both NO_3^- removal efficiencies and NO_3^- removal rates have increased with temperature. The bioreactor efficiency doubled in term of NO_3^- removal compared to the previous year showing an average value of 65%. Similarly, rate was positively related to temperature.

Moreover, it seems that a positive effect of heating was also noted on both hydrolysis and bacterial growth. As a result, organic carbon (TOC) and nutrients (phosphorus compounds) were released and made accessible for the bacteria to perform denitrification. The bacteria community increased, and this change was significantly related to temperature for the first section of the bioreactor which underwent the main temperatures variations. As more bacteria were present, denitrification was enhanced as well. Therefore, temperature effects on hydrolysis and bacteria growth are in turn beneficial for denitrification and improve NO_3^- removal.

These results were achieved even though flow and temperature propagation were not constant along the bioreactor. To accomplish greater NO_3^- removal, the preferential flow path should be investigated and if possible eliminated, and a stable temperature gradient should be implemented.

Finally, the heating operational cost could represent an issue if more bioreactors possessing a heating device are projected to be constructed. A solution that could be investigated to reduce this cost while achieving good NO_3^- removal would be to warm the bioreactor via a “heat-pulse”. In fact, a potential long-lasting heating effect on denitrification was observed where, after a period of two months without heating, NO_3^- removal efficiency reached a plateau above of 45% similar to the one obtained during heating.

To conclude, even if some uncertainties remain, this study has been an encouraging first approach into the use of a heater to enhance denitrification rates. It could represent a solution for the future of sustainable mining and nitrogen leaching in extreme climates such as Kiruna.

8 Acknowledgements

My thesis would not have been possible without the financial support of LKAB which is gratefully acknowledged. Through this project, I had the opportunity to stay in Kiruna for a period of one month to sharpen my background knowledge on the LKAB iron ore mine, specifically on their denitrifying bioreactors (DBR). It also permitted me to manage and operate the DBR analysis and have a great introduction to this working environment. Although the weather was sometimes discouraging to achieve my field work, the support provided by LKAB employees, the fika breaks and the fantastic auroras kept me determined and motivated. I am especially grateful to Roger Herbert without whom this project would have never been possible, Tomas Salmi for the assistance with my field work, Mattias Ylipää for his guidance and introduction of the LKAB mine company, Maximilian Körtge for his help during my project and Christian Zdanowicz for his precious feedback on my report.

I also want to address a special thanks to Sofia Papadopoulou and Christoffer Begvall that helped me with laboratory work with the quantification of the bacterial community and with the analysis of TOC and phosphorus compounds.

Finally, I'd like to extend my gratitude to all the people that have been involved in the NITREM project. Their collected data and research have been a major help in my understanding of woodchips denitrifying bioreactor systems.

9 References

Addy, K., Gold, A.J., Christianson, L.E., David, M.B., Schipper, L.A. & Ratigan, N.A. (2016). Denitrifying Bioreactors for Nitrate Removal: A Meta-Analysis. *Journal of Environmental Quality*, 45 (3), 873–881. https://doi.org/10.2134/jeq2015.07.0399

Arcus, V.L., Prentice, E.J., Hobbs, J.K., Mulholland, A.J., Van der Kamp, M.W., Pudney, C.R., Parker, E.J. & Schipper, L.A. (2016). On the Temperature Dependence of Enzyme-Catalyzed Rates. *Biochemistry*, 55 (12), 1681–1688. https://doi.org/10.1021/acs.biochem.5b01094

Asghari, F.S. & Yoshida, H. (2010). Conversion of Japanese red pine wood (Pinus densiflora) into valuable chemicals under subcritical water conditions. *Carbohydrate Research*, 345 (1), 124–131. https://doi.org/10.1016/j.carres.2009.10.006

Bailey, B.L., Smith, L.J.D., Blowes, D.W., Ptacek, C.J., Smith, L. & Sego, D.C. (2013). The Diavik Waste Rock Project: Persistence of contaminants from blasting agents in waste rock effluent. *Applied Geochemistry*, 36, 256–270. https://doi.org/10.1016/j.apgeochem.2012.04.008

Bear, J. (1988). *Dynamics of Fluids in Porous Media*. Courier Corporation.

Bothe, H., Ferguson, S. & Newton, W.E. (2006). *Biology of the Nitrogen Cycle*. Elsevier.

Burgin, A.J. & Hamilton, S.K. (2007). Have we overemphasized the role of denitrification in aquatic ecosystems? A review of nitrate removal pathways. *Frontiers in Ecology and the Environment*, 5 (2), 89–96. https://doi.org/10.1890/1540-9295(2007)5[89:HWOTRO]2.0.CO;2

Cameron, S.G. & Schipper, L.A. (2010). Nitrate removal and hydraulic performance of organic carbon for use in denitrification beds. *Ecological Engineering*, 36 (11), 1588–1595. https://doi.org/10.1016/j.ecoleng.2010.03.010

Canfield, D.E., Glazer, A.N. & Falkowski, P.G. (2010). The evolution and future of Earth's nitrogen cycle. *Science (New York, N.Y.)*, 330 (6001), 192–196. https://doi.org/10.1126/science.1186120

Chandrasekaran, S.R., Hopke, P.K., Rector, L., Allen, G. & Lin, L. (2012). Chemical Composition of Wood Chips and Wood Pellets. *Energy & Fuels*, 26 (8), 4932–4937. https://doi.org/10.1021/ef300884k

Christianson, L., Helmers, M., Bhandari, A. & Moorman, T. (2013). Internal hydraulics of an agricultural drainage denitrification bioreactor. *Ecological Engineering*, 52, 298–307. https://doi.org/10.1016/j.ecoleng.2012.11.001

Chung, S.-O. & Horton, R. (1987). Soil heat and water flow with a partial surface mulch. *Water Resources Research*, 23 (12), 2175–2186. https://doi.org/10.1029/WR023i012p02175

Clark, G. (1981). Basic properties of ammonium nitrate fuel oil explosive (ANFO). *Basic properties ofammonium nitrate fuel oil explosive (ANFO),*

Davis, M.P., Martin, E.A., Moorman, T.B., Isenhart, T.M. & Soupir, M.L. (2019). Nitrous oxide and methane production from denitrifying woodchip bioreactors at three hydraulic residence times. *Journal of Environmental Management*, 242, 290–297. https://doi.org/10.1016/.jenvman.2019.04.055

Feyereisen, G.W., Moorman, T.B., Christianson, L.E., Venterea, R.T., Coulter, J.A. & Tschirner, U.W. (2016). Performance of Agricultural Residue Media in Laboratory Denitrifying Bioreactors at Low Temperatures. *Journal of Environmental Quality*, 45 (3), 779–787. https://doi.org/10.2134/jeq2015.07.0407

Forsyth, B., Cameron, A. & Miller, S. (1995). Explosive and water quality. *Proceedings of Sudbury '95 Mining and the Environment, Montreal, Quebec, Canada: MEND (Mine Environment Neutral Drainage)*, 795–803

Gasol, J.M. & Giorgio, P.A. del (2000). Using flow cytometry for counting natural planktonic bacteria and understanding the structure of planktonic bacterial communities. *Scientia Marina*, 64 (2), 197–224. https://doi.org/10.3989/scimar.2000.64n2197

Gerke, H.H. (2006). Preferential flow descriptions for structured soils. *Journal of Plant Nutrition and Soil Science*, 169 (3), 382–400. https://doi.org/10.1002/jpln.200521955

Ghane, E., Fausey, N.R. & Brown, L.C. (2015). Modeling nitrate removal in a denitrification bed. *Water Research*, 71, 294–305. https://doi.org/10.1016/j.watres.2014.10.039

Halling-Sørensen, B. & Jorgensen, S.E. (1993). *The Removal of Nitrogen Compounds from Wastewater*. Elsevier.

Häyrynen, K., Pongrácz, E., Väisänen, V., Pap, N., Mänttäri, M., Langwaldt, J. & Keiski, R.L. (2009). Concentration of ammonium and nitrate from mine water by reverse osmosis and nanofiltration. *Desalination*, 240 (1), 280–289. https://doi.org/10.1016/j.desal.2008.02.027

Healy, M.G., Ibrahim, T.G., Lanigan, G.J., Serrenho, A.J. & Fenton, O. (2012). Nitrate removal rate, efficiency and pollution swapping potential of different organic carbon media in laboratory denitrification bioreactors. *Ecological Engineering*, 40, 198–209. https://doi.org/10.1016/j.ecoleng.2011.12.010

Herbert, R. (2019). *Deliverable D3.2.2 Evaluation of sensor performance*. EIT RawMaterials project NITREM (non published data).

Herbert, R. (2020a). *Combined deliberable D3.2.3 Water quality results from second sampling season and D.2.4 Water quality results from third sampling season. Water quality results from 2018-2020.* EIT RawMaterials project NITREM (non published data).

Herbert, R. (2020b). *Deliverable D2.2.1 Description of bioreactor and water collection system design and construction*. EIT RawMaterials project NITREM (non published data).

Herbert, R. (2022). *Deliverable D3.2.5 Water quality results from 2018-2021*. EIT RawMaterials project NITREM (non published data).

Herbert, R.B., Winbjörk, H., Hellman, M. & Hallin, S. (2014). Nitrogen removal and spatial distribution of denitrifier and anammox communities in a bioreactor for mine drainage treatment. *Water Research*, 66, 350–360. https://doi.org/10.1016/j.watres.2014.08.038

Hunter, W.J. (2003). Accumulation of nitrite in denitrifying barriers when phosphate is limiting. *Journal of Contaminant Hydrology*, 66 (1), 79–91. https://doi.org/10.1016/S0169-7722(03)00008-1

Ibanez, J.G., Hernandez-Esparza, M., Doria-Serrano, C., Fregoso-Infante, A. & Singh, M.M. (2008). Alkalinity and Buffering Capacity of Water. In: Ibanez, J.G., Hernandez-Esparza, M., Doria-Serrano, C., Fregoso-Infante, A., & Singh, M.M. (eds.) *Environmental Chemistry: Microscale Laboratory Experiments*. New York, NY: Springer, 28–56. https://doi.org/10.1007/978-0-387-49493-7_3

Iranmahboob, J., Nadim, F. & Monemi, S. (2002). Optimizing acid-hydrolysis: a critical step for production of ethanol from mixed wood chips. *Biomass and Bioenergy*, 22 (5), 401–404. https://doi.org/10.1016/S0961-9534(02)00016-8

Kaviany, M. (2012). *Principles of Heat Transfer in Porous Media*. Springer Science & Business Media.

Kiani, S., Lehosmaa, K., Kløve, B. & Ronkanen, A.-K. (2022). Nitrogen removal of mine-influenced water in a hybrid bioreactor with floating hook-moss (Warnstorfia fluitans) in cold climate conditions. *Ecological Engineering*, 177, 106562. https://doi.org/10.1016/j.ecoleng.2022.106562

Lebaron, P., Parthuisot, N. & Catala, P. (1998). Comparison of Blue Nucleic Acid Dyes for Flow Cytometric Enumeration of Bacteria in Aquatic Systems. *Applied and Environmental Microbiology*, 64 (5), 1725–1730. https://doi.org/10.1128/AEM.64.5.1725-1730.1998

Liu, Y. & von Wirén, N. (2017). Ammonium as a signal for physiological and morphological responses in plants. *Journal of Experimental Botany*, 68 (10), 2581–2592. https://doi.org/10.1093/jxb/erx086

LKAB (2016). *Miljörapport LKAB Kiruna 2015 [Environmental Report LKAB Kiruna 2015]*. Luossavaara-Kiirunavaara AB. (in Swedish).

LKAB (2017). *It starts with the iron*. *LKAB*. https://www.lkab.com/en/about-lkab/lkab-in-brief/it-starts-with-the-iron/ [2022-03-29]

Maxwell, B., Díaz-García, C., Martínez-Sánchez, J.J., Birgand, F. & Álvarez-Rogel, J. (2020). Temperature sensitivity of nitrate removal in woodchip bioreactors increases with woodchip age and following drying-rewetting cycles. *Environmental Science: Water Research & Technology*, 6. https://doi.org/10.1039/D0EW00507J

Morin, K.A. & Hutt, N.M. (2009). Mine-Water Leaching of Nitrogen Species from Explosive Residues. Proceedings of GeoHalifax, 20–24.

Murphy, J. & Riley, J.P. (1962). A modified single solution method for the determination of phosphate in natural waters. *Analytica Chimica Acta*, 27, 31–36. https://doi.org/10.1016/S0003-2670(00)88444-5

Ng, A.N.L. & Kim, A.S. (2007). A mini-review of modeling studies on membrane bioreactor (MBR) treatment for municipal wastewaters. *Desalination*, 212 (1), 261–281. https://doi.org/10.1016/j.desal.2006.10.013

Ni, S.-Q. & Zhang, J. (2013). Anaerobic Ammonium Oxidation: From Laboratory to Full-Scale Application. *BioMed research international*, 2013, 469360. https://doi.org/10.1155/2013/469360

NITREM (n.d.). https://nitrem.eu/ [2022-05-15]

Nordström, A. (2014). *Denitrification in a Low Temperature Bioreactor System - Laboratory column studies*. Uppsala Universitet. https://www.diva-portal.org/smash/get/diva2:726515/FULLTEXT01.pdf

Nordström, A. (2019). *Biogeochemical Processes in Denitrifying Woodchip Bioreactors and their Application in the Mining Industry*. Uppsala Universitet. http://uu.diva-portal.org/smash/record.jsf?aq2=%5B%5B%5D%5D&c=3&af=%5B%5D&searchType=LIST_COMING&sortOrder2=title_sort_asc&query=&language=en&pid=diva2%3A1299616&aq=%5B%5B%5D%5D&sf=all&aqe=%5B%5D&sortOrder=author_sort_asc&onlyFullText=false&noOfRows=50&dswid=1811

Nordström, A., Hellman, M., Hallin, S. & Herbert, R.B. (2021). Microbial controls on net production of nitrous oxide in a denitrifying woodchip bioreactor. *Journal of Environmental Quality*, 50 (1), 228–240. https://doi.org/10.1002/jeq2.20181

Nordström, A. & Herbert, R.B. (2018). Determination of major biogeochemical processes in a denitrifying woodchip bioreactor for treating mine drainage. *Ecological Engineering*, 110, 54–66. https://doi.org/10.1016/j.ecoleng.2017.09.018

Nordström, A. & Herbert, R.B. (2019). Identification of the temporal control on nitrate removal rate variability in a denitrifying woodchip bioreactor. *Ecological Engineering*, 127, 88–95. https://doi.org/10.1016/j.ecoleng.2018.11.015

Pandey, C.B., Kumar, U., Kaviraj, M., Minick, K.J., Mishra, A.K. & Singh, J.S. (2020). DNRA: A short-circuit in biological N-cycling to conserve nitrogen in terrestrial ecosystems. *Science of The Total Environment*, 738, 139710. https://doi.org/10.1016/j.scitotenv.2020.139710

PBS (n.d.). *Thermo Fischer Scientific*. https://www.thermofisher.com/se/en/home/life-science/cell-culture/mammalian-cell-culture/reagents/balanced-salt-solutions.html [2022-06-14]

Prasad, V., Kulacki, F.A. & Keyhani, M. (1985). Natural convection in porous media. *Journal of Fluid Mechanics*, 150, 89–119. https://doi.org/10.1017/S0022112085000040

Rahman, M., Grace, M.R., Roberts, K.L., Kessler, A.J. & Cook, P.L.M. (2019). Effect of temperature and drying-rewetting of sediments on the partitioning between denitrification and DNRA in constructed urban stormwater wetlands. *Ecological Engineering*, 140, 105586. https://doi.org/10.1016/j.ecoleng.2019.105586

Robertson, W.D. (2010). Nitrate removal rates in woodchip media of varying age. *Ecological Engineering*, 36 (11), 1581–1587. https://doi.org/10.1016/j.ecoleng.2010.01.008

Schipper, L.A., Hobbs, J.K., Rutledge, S. & Arcus, V.L. (2014). Thermodynamic theory explains the temperature optima of soil microbial processes and high Q10 values at low temperatures. *Global Change Biology*, 20 (11), 3578–3586. https://doi.org/10.1111/gcb.12596

Schipper, L.A., Robertson, W.D., Gold, A.J., Jaynes, D.B. & Cameron, S.C. (2010). Denitrifying bioreactors—An approach for reducing nitrate loads to receiving waters. *Ecological Engineering*, 36 (11), 1532–1543. https://doi.org/10.1016/j.ecoleng.2010.04.008

Schlesinger, W.H. & Bernhardt, E.S. (2020). The Atmosphere. *Biogeochemistry*, 51–97. https://doi.org/10.1016/B978-0-12-814608-8.00003-7

Sharrer, K.L., Christianson, L.E., Lepine, C. & Summerfelt, S.T. (2016). Modeling and mitigation of denitrification 'woodchip' bioreactor phosphorus releases during treatment of aquaculture wastewater. *Ecological Engineering*, 93, 135–143. https://doi.org/10.1016/j.ecoleng.2016.05.019

Shiskowski, D.M. & Mavinic, D.S. (1998). Biological treatment of a high ammonia leachate: influence of external carbon during initial startup. *Water Research*, 32 (8), 2533–2541. https://doi.org/10.1016/S0043-1354(97)00465-X

Stumm, W. & Morgan, J.J. (2012). *Aquatic Chemistry: Chemical Equilibria and Rates in Natural Waters*. John Wiley & Sons.

Sun, Y. & Cheng, J. (2002). Hydrolysis of lignocellulosic materials for ethanol production: a review. *Bioresource Technology*, 83 (1), 1–11. https://doi.org/10.1016/S0960-8524(01)00212-7

Takenaka, N., Takahashi, I., Suekane, H., Yamamoto, K., Sadanaga, Y. & Bandow, H. (2011). Acceleration of Ammonium Nitrite Denitrification by Freezing: Determination of Activation Energy from the Temperature of Maximum Reaction Rate. *The Journal of Physical Chemistry A*, 115 (50), 14446–14451. https://doi.org/10.1021/jp2093466

Trenberth, K.E. & Guillemot, C.J. (1994). The total mass of the atmosphere. *Journal of Geophysical Research: Atmospheres*, 99 (D11), 23079–23088. https://doi.org/10.1029/94JD02043

Warneke, S., Schipper, L.A., Matiasek, M.G., Scow, K.M., Cameron, S., Bruesewitz, D.A. & McDonald, I.R. (2011). Nitrate removal, communities of denitrifiers and adverse effects in different carbon substrates for use in denitrification beds. *Water Research*, 45 (17), 5463–5475. https://doi.org/10.1016/j.watres.2011.08.007

Wilderer, P.A., Jones, W.L. & Dau, U. (1987). Competition in denitrification systems affecting reduction rate and accumulation of nitrite. *Water Research*, 21 (2), 239–245. https://doi.org/10.1016/0043-1354(87)90056-X

Zaitsev, G., Mettänen, T. & Langwaldt, J. (2008). Removal of ammonium and nitrate from cold inorganic mine water by fixed-bed biofilm reactors. *Minerals Engineering*, 21 (1), 10–15. https://doi.org/10.1016/j.mineng.2007.08.014

Zumft, W.G. (1997). Cell biology and molecular basis of denitrification. *Microbiology and Molecular Biology Reviews*, 61 (4), 533–616. https://doi.org/10.1128/mmbr.61.4.533-616.1997

Appendix A: Temperatures used for plotting

A.1 2019 and 2020

The temperatures taken during 2019 and 2020 for the profile sampling come from the permanent sensors. These values were used for nitrate removal rate graphical estimations (further explained in appendix E). Since no heating system was implemented during this time, no temperature variations were noticeable, and the average was assumed to define the temperature within the bioreactor (table A1).

Table A1. Sensor's temperature for 2019 and 2020.

Date	**Temperature(°C)**				
	T1	T2	T3	T4	Mean
20 Jun 19	2.97	3.13	2.94	2.97	3.00
24 Jun 19	3.24	2.94	2.91	3.22	3.08
02 Jul 19	3.46	4.18	4.26	4.11	4.00
05 Jul 19	3.25	3.61	3.68	4.12	3.66
25 Jul 19	2.65	2.63	2.63	2.87	2.70
17 Jun 20	2.88	2.47	2.28	3.07	2.68
22 Jun 20	3.14	3.06	2.53	2.62	2.84
29 Jun 20	3.98	5.37	4.53	3.16	4.26
07 Jul 20	4.42	5.18	4.54	4.00	4.53
13 Jul 20	5.51	5.22	4.75	4.50	4.99

A.2 2022

A-wells were not covered by sensors; thus, the manual measurements were considered for further analysis (table A2).

Table A2. Temperature (°C) values taken from manual measurements used for the sampling profile A-wells.

Date	**Temperature (°C)**						
	Inlet	P1A	P2A	P3A	P4A	P5A	Outlet
29-Mar-22	3.40	4.30	4.60	5.00	5.40	4.40	4.30
19-Apr-22	26.90	26.40	14.00	4.80	5.10	4.80	4.40
26-Apr-22	4.10	18.10	16.40	10.80	11.40	3.20	6.20

Since temperature was not continuously measured in wells P2B, P3B and P4B, it was estimated from near-lying measurements given by both permanent (T1, T2, T3, T4) and mobile sensors (Tinlet, T1B, T3B, T5B) as seen in figure A1. The results are shown in table A3 and, similarly to the previous section, were used for nitrate removal rate graphical estimations (further explained in appendix E).

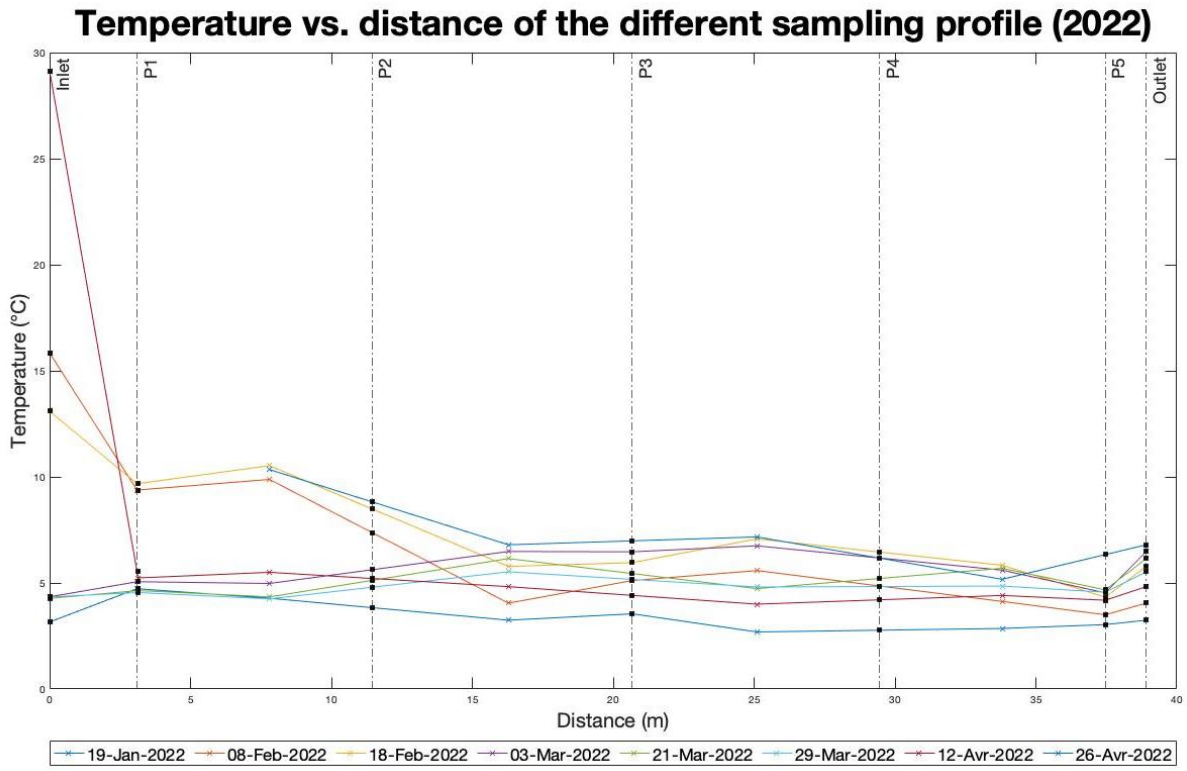

Figure A1. Graphical estimation of B-wells temperatures. The crosses indicate sensors measurements while the dots represent the estimated values by linear interpolation.

Table A3. Estimated temperatures of B-wells during sampling profile events. Since the mobile sensors were removed from B-wells the 19th of April, the temperature of the 26th of April could not be estimated for the inlet and P1B. Therefore, they were replaced by manual measurements values (italic) as they were evaluated to be acceptable (see figure A.2).

Date	**Temperature (°C)**						
	Inlet	P1B	P2B	P3B	P4B	P5B	Outlet
19-Jan-22	3.16	4.73	3.84	3.55	2.77	3.04	3.25
08-Feb-22	15.84	9.38	7.38	5.11	4.85	3.50	4.05
18-Feb-22	13.10	9.68	8.49	5.96	6.45	4.33	5.78
03-Mar22	4.35	5.06	5.62	6.47	6.17	4.54	6.48
21-Mar-22	4.27	4.64	5.12	5.44	5.21	4.68	6.15
29-Mar22	4.34	4.55	4.80	5.17	4.83	4.56	5.53
12-Apr-22	29.13	5.54	5.21	4.41	4.21	4.19	4.83
26-Apr-22	4.10	10.20	8.82	6.98	6.17	6.34	6.80

A correlation analysis was run between these results and the manual measurements for the last three sampling profiles to see if they could be used for further investigation. Overall, B-wells values estimations did not show any major difference with the manual measurements with a correlation coefficient of 84.2% (figure A2). Therefore, these values were considered acceptable for further analysis.

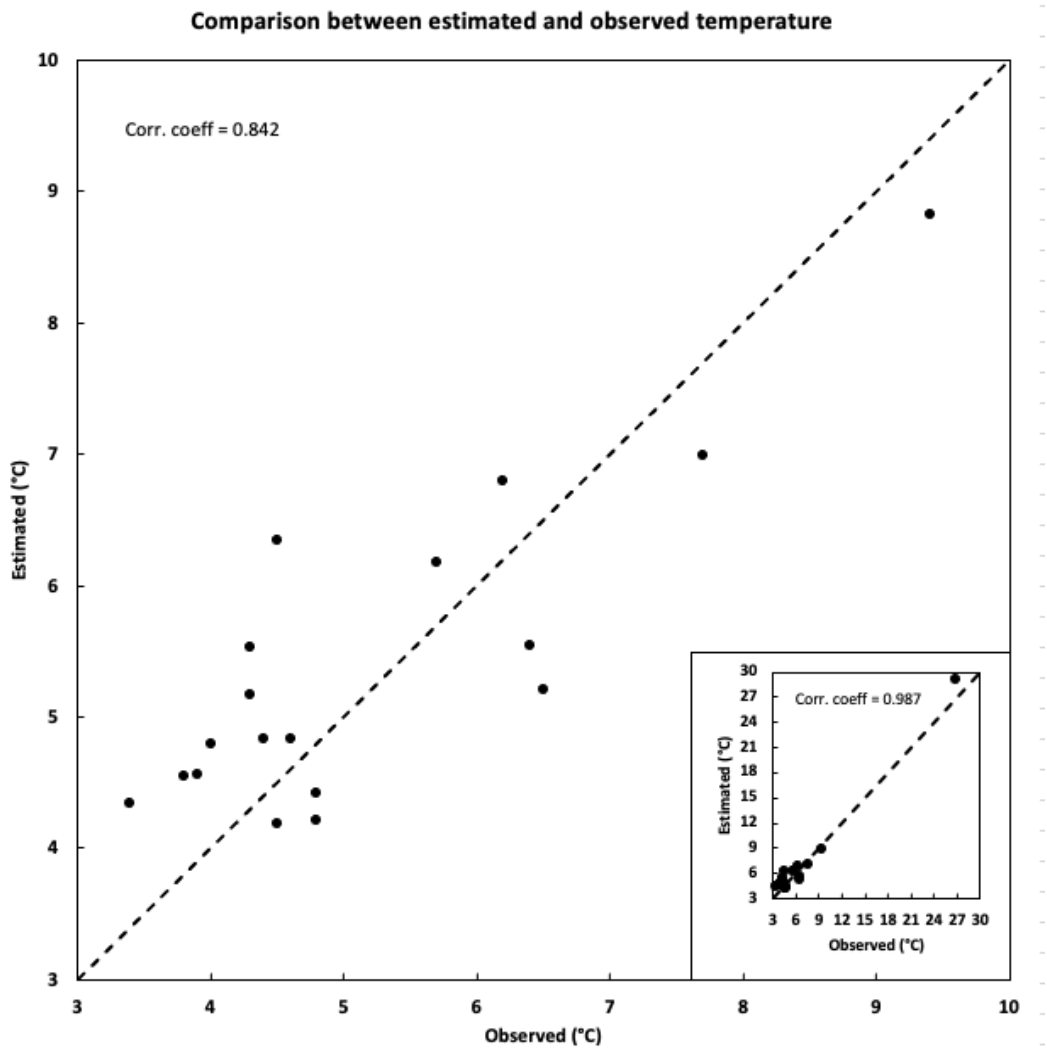

Figure A2. Correlation analysis between estimated and observed (manual measurements) temperature values for the last three sampling profile of B-wells. The dashed line represents the 1:1 line. On the bottom right corner, the extreme temperature value was considered and give a correlation coefficient of 98.7% while the overall picture excluded this point to give a correlation coefficient of 84.2%.

Appendix B: Sampling profile information

The sampling profiles were performed approximately every two weeks. Detailed information on the date and the person that performed the field work are presented in the table below.

Table B1. Date and person performing the profile sampling during the study period.

When?	Who?
19 Jan 22 08 Feb 22 18 Feb 22 03 Mar22	Laura Nina Bettoni
21 Mar22 29 Mar22 12 Apr 22 26 Apr 22	Tomas Salmi LKAB personnel

Appendix C: Chemical analysis results

C.1 Nitrogen compounds

C.1.1 Nitrate

Nitrate was analyzed during all sampling years (2019, 2020, 2022) for both A and B wells (tables C1-C3).

Table C1. Nitrate concentrations from profile sampling performed in 2019. For A- (above) and B-wells (below).

Date	Inlet (mg L^{-1} N)	P1A (mg L^{-1} N)	P2A (mg L^{-1} N)	P3A (mg L^{-1} N)	P4A (mg L^{-1} N)	P5A (mg L^{-1} N)	Outlet (mg L^{-1} N)
20 Jun 19	63.36	51.92	36.19	7.04	1.24	0.32	0.24
24 Jun 19	30.47	25.52	21.23	11.00	0.35	0.45	0.49
02 Jul 19	48.00	25.60	1.81	2.91	<0.015	0.33	N/A
05 Jul 19	62.00	29.00	21.30	0.24	<0.015	0.27	N/A
25 Jul 19	69.00	46.90	24.50	6.33	<0.015	0.28	N/A

Date	Inlet (mg L^{-1} N)	P1B (mg L^{-1} N)	P2B (mg L^{-1} N)	P3B (mg L^{-1} N)	P4B (mg L^{-1} N)	P5B (mg L^{-1} N)	Outlet (mg L^{-1} N)
20 Jun 19	63.36	59.29	18.37	2.71	0.23	0.42	0.24
24 Jun 19	30.47	29.59	18.15	0.23	0.23	0.49	0.49
02 Jul 19	48.00	43.90	3.30	<0.015	<0.015	<0.015	N/A
05 Jul 19	62.00	57.20	14.50	<0.015	<0.015	0.33	N/A
25 Jul 19	69.00	65.80	26.20	1.87	<0.015	0.32	N/A

Table C2. Nitrate concentrations from profile sampling performed in 2020. For A- (above) and B-wells (below).

Date	Inlet (mg L^{-1} N)	P1A (mg L^{-1} N)	P2A (mg L^{-1} N)	P3A (mg L^{-1} N)	P4A (mg L^{-1} N)	P5A (mg L^{-1} N)	Outlet (mg L^{-1} N)
17 Jun 20	35.86	32.67	31.79	N/A	N/A	N/A	14.96
22 Jun 20	46.86	38.17	35.75	24.86	21.23	7.04	15.73
29 Jun 20	49.83	48.84	46.2	25.96	17.6	2.64	12.21
07 Jul 20	29.26	40.48	46.53	35.31	15.84	0.74	10.45
13 Jul 20	26.40	52.80	38.28	20.24	14.52	1.56	8.20

Date	Inlet (mg L^{-1} N)	P1B (mg L^{-1} N)	P2B (mg L^{-1} N)	P3B (mg L^{-1} N)	P4B (mg L^{-1} N)	P5B (mg L^{-1} N)	Outlet (mg L^{-1} N)
17 Jun 20	35.86	39.60	32.67	N/A	N/A	N/A	14.96
22 Jun 20	46.86	44.44	31.79	25.08	11.44	9.79	15.73
29 Jun 20	49.83	46.97	32.12	11.00	5.50	8.14	12.21
07 Jul 20	29.26	30.47	32.89	14.19	0.26	0.70	10.45
13 Jul 20	26.40	53.02	25.30	16.06	0.72	1.21	8.20

Table C3. Nitrate concentrations from profile sampling performed in 2022. For A- (above) and B-wells (below).

Date	Inlet (mg L^{-1} N)	P1A (mg L^{-1} N)	P2A (mg L^{-1} N)	P3A (mg L^{-1} N)	P4A (mg L^{-1} N)	P5A (mg L^{-1} N)	Outlet (mg L^{-1} N)
18 Feb 22	85.80	76.89	59.18	N/A	N/A	N/A	42.57
03 Mar22	90.09	85.14	58.85	15.07	14.19	N/A	23.10
21 Mar22	79.09	39.38	57.42	52.03	40.37	16.28	25.08
29 Mar22	81.73	32.01	77.44	55.88	52.80	30.91	41.14
12 Apr 22	70.95	41.14	34.43	36.74	31.46	16.28	18.59
26 Apr 22	47.63	19.69	<0.015	<0.015	<0.015	7.04	6.82

Date	Inlet (mg L^{-1} N)	P1B (mg L^{-1} N)	P2B (mg L^{-1} N)	P3B (mg L^{-1} N)	P4B (mg L^{-1} N)	P5B (mg L^{-1} N)	Outlet (mg L^{-1} N)
19 Jan 22	99.99	117.48	100.21	75.68	4.62	2.64	15.40
08 Feb 22	49.94	23.10	39.71	26.51	45.98	41.80	44.33
18 Feb 22	85.80	45.10	36.74	28.82	25.74	30.47	42.57
03 Mar22	90.09	89.43	88.44	0.18	<0.015	8.03	23.10
21 Mar22	79.09	70.62	72.38	55.99	33.00	<0.015	25.08
29 Mar22	81.73	66.55	57.20	55.22	38.28	<0.015	41.14
12 Apr 22	70.95	81.73	36.96	54.34	30.58	0.27	18.59
26 Apr 22	47.63	45.21	29.37	24.64	24.31	0.36	6.82

C.1.2 Nitrite and ammonium

Nitrite (table C4) and ammonium (table C5) were only considered for the profile sampling of 2022.

Table C4. Nitrite concentrations from profile sampling performed in 2022. For A- (above) and B-wells (below).

Date	Inlet (mg L^{-1} N)	P1A (mg L^{-1} N)	P2A (mg L^{-1} N)	P3A (mg L^{-1} N)	P4A (mg L^{-1} N)	P5A (mg L^{-1} N)	Outlet (mg L^{-1} N)
18 Feb 22	<0.015	<0.015	<0.015	N/A	N/A	N/A	1.188
03 Mar22	<0.015	<0.015	<0.015	<0.015	0.396	N/A	1.133
21 Mar22	<0.015	<0.015	<0.015	<0.015	0.22	0.792	0.715
29 Mar22	<0.015	<0.015	<0.015	<0.015	0.253	1.947	0.748
12 Apr 22	0.075	0.016	0.043	<0.015	<0.015	0.913	0.264
26 Apr 22	<0.015	<0.015	<0.015	<0.015	<0.015	0.462	0.649

Date	Inlet (mg L^{-1} N)	P1B (mg L^{-1} N)	P2B (mg L^{-1} N)	P3B (mg L^{-1} N)	P4B (mg L^{-1} N)	P5B (mg L^{-1} N)	Outlet (mg L^{-1} N)
19 Jan 22	<0.015	<0.015	<0.015	0.308	<0.015	<0.015	0.187
08 Feb 22	<0.015	<0.015	<0.015	0.264	1.771	2.079	0.616
18 Feb 22	<0.015	<0.015	<0.015	1.265	3.883	8.72	1.188
03 Mar22	<0.015	<0.015	<0.015	<0.015	<0.015	10	1.133
21 Mar22	<0.015	<0.015	<0.015	0.539	2.574	<0.015	0.715
29 Mar22	<0.015	<0.015	<0.015	0.594	1.892	<0.015	0.748
12 Apr 22	0.075	<0.015	<0.015	0.528	2.552	<0.015	0.264
26 Apr 22	<0.015	<0.015	<0.015	1.243	2.915	0.016	0.649

Table C5 Ammonium concentrations from profile sampling performed in 2022. For A- (above) and B-wells (below).

Date	Inlet (mg L^{-1} N)	P1A (mg L^{-1} N)	P2A (mg L^{-1} N)	P3A (mg L^{-1} N)	P4A (mg L^{-1} N)	P5A (mg L^{-1} N)	Outlet (mg L^{-1} N)
18 Feb 22	<0.015	<0.015	<0.015	N/A	N/A	N/A	0.298
03 Mar22	<0.015	0.198	1.1	1.029	0.844	N/A	0.765
21 Mar22	<0.015	0.159	0.402	0.677	1.202	1.052	1.176
29 Mar22	<0.015	0.234	0.213	0.593	0.698	0.854	0.925
12 Apr 22	<0.015	0.436	0.39	0.243	0.428	0.417	0.317
26 Apr 22	<0.015	<0.015	0.884	1.116	0.954	0.17	0.017

Date	Inlet (mg L^{-1} N)	P1B (mg L^{-1} N)	P2B (mg L^{-1} N)	P3B (mg L^{-1} N)	P4B (mg L^{-1} N)	P5B (mg L^{-1} N)	Outlet (mg L^{-1} N)
19 Jan 22	0.045	0.095	0.082	0.692	0.473	0.789	0.041
08 Feb 22	<0.015	0.416	0.546	0.307	0.318	<0.015	<0.015
18 Feb 22	<0.015	0.595	0.519	<0.015	0.049	0.328	0.298
03 Mar22	<0.015	0.091	0.753	1.14	1.019	0.509	0.765
21 Mar22	<0.015	0.055	0.491	0.816	1.27	1.196	1.176
29 Mar22	<0.015	0.068	0.471	0.757	1.409	1.395	0.925
12 Apr 22	<0.015	0.153	0.151	0.255	0.224	0.048	0.317
26 Apr 22	<0.015	1.096	0.878	0.628	0.41	1.117	0.017

C.2 Total phosphorus and total organic carbon

Total phosphorus (table C6) and total organic carbon (table C7) were analyzed for the B-wells of the profile sampling of 2022.

Table C6. Total phosphorus concentrations for the B-wells of profile sampling performed in 2022.

Date	P1B (µg L^{-1} P)	P2B (µg L^{-1} P)	P3B (µg L^{-1} P)	P4B (µg L^{-1} P)	P5B (µg L^{-1} P)
21-Mar	5	12	20	37	26
29-Mar	17	15	18	34	24
12-Apr	16	28	24	21	48
26-Apr	28	54	46	55	47

Table C7. Total organic carbon concentrations for the B-wells of profile sampling performed in 2022.

Date	P1B (mg L^{-1} C)	P2B (mg L^{-1} C)	P3B (mg L^{-1} C)	P4B (mg L^{-1} C)	P5B (mg L^{-1} C)
21-Mar-22	3.07	3.71	4.36	5.57	7.55
29-Mar-22	3.15	4.85	4.10	5.08	8.42
12-Apr-22	3.94	3.42	4.19	4.02	6.71
26-Apr-22	10.0	7.22	7.28	6.62	6.66

Appendix D: Bacterial abundance results

The microbial abundance values are shown in the table below (table D1). Note that the values for the 18th of February and the 3rd of March were not taken into consideration.

D1. Bacterial abundance. The values obtained from the 18th of February and the 3rd of March were not considered as an important loss has been observed due to unfavorable preservation conditions.

Date	Inlet (events mL^{-1})	P1B (events mL^{-1})	P2B (events mL^{-1})	P3B (events mL^{-1})	P4B (events mL^{-1})	P5B (events mL^{-1})	Outlet (events mL^{-1})
19-Jan-22	1107200	1435627	5768853	9124373	17664640	19331307	25677440
08-Feb-22	6978560	5258667	17585707	24386453	20803520	23770347	16685013
18-Feb-22	307200	6106453	7394240	8030933	6024640	8738987	4510613
03-Mar-22	1038400	871200	3481760	8925440	19382933	16480853	14836693
21-Mar-22	2480853	1076800	4017600	24702400	37726507	41264107	19038827
29-Mar-22	1939840	2563413	8526613	11080640	27316800	33084373	19800107
12-Apr-22	283200	5355200	6547947	9065280	9230507	16887147	20307947
26-Apr-22	1730133	9134080	27090667	32584427	20745920	20200320	13484587

Appendix E: Nitrate removal rate: steps included in the graphical estimation

E.1 Calibration curve between flow rate and velocity

The calibration curve between velocities, determined from electrical conductivity measurements, and matching flow rate is linear and equal to y= 0.0003x – 1.112 with a R^2 value of 91.1% (figure E1).

The velocities were estimated for each sampling period based on their corresponding average flow rate (table E1). Then, the cumulative time can be calculated (equation 7). Compared to 2019, the velocity in 2022 is lower by an order of magnitude.

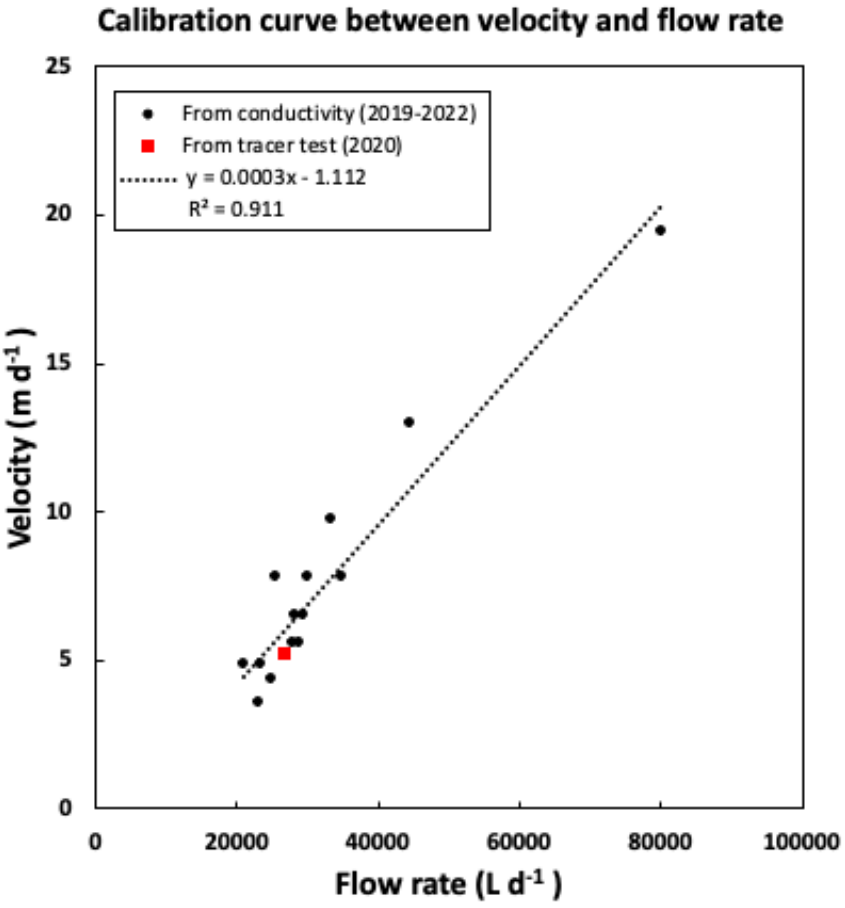

Figure E1. Calibration curve between flow rate and velocity.

Table E1. Estimated velocity values for the three different profile sampling periods.

Year	Period	Average flow rate (L d^{-1})	Corresponding velocity (m d^{-1})*
2019	20 Jun to 25 Jul	39 860	10.85
2020	17 Jun to 13 Jul	24 777	6.32
2022	20 Jan to 26 Apr	10 093	1.92

*The corresponding velocity was determined by using the model equation in figure E.1.

E.2 Nitrate removal rates by grouping approach

The nitrate removal rates were first estimated through the grouping approach. This means that all profiles within the period were used. For 2019, both nitrate concentrations (0^{th} order rate law) and ln nitrate concentrations (1^{st} order rate law) were plotted against time. No major distinction was observed between the 1^{st} and the 0^{th} order rate law as R^2 were high and rather similar (figure E2). However, as seen in section E3, by using the individual approach, the 1^{st} order rate law seems to better fit the data (figure E.5) and therefore was considered to estimate the nitrate removal rate in this case as well.

In contrast, both 2020 and 2022 showed distinctive better results while being fit by a 0^{th} than a 1^{st} order rate law which is why only the 0^{th} order rate law is presented in this case (figure E3 and E4). The obtained nitrate removal rates are summarized in table E2.

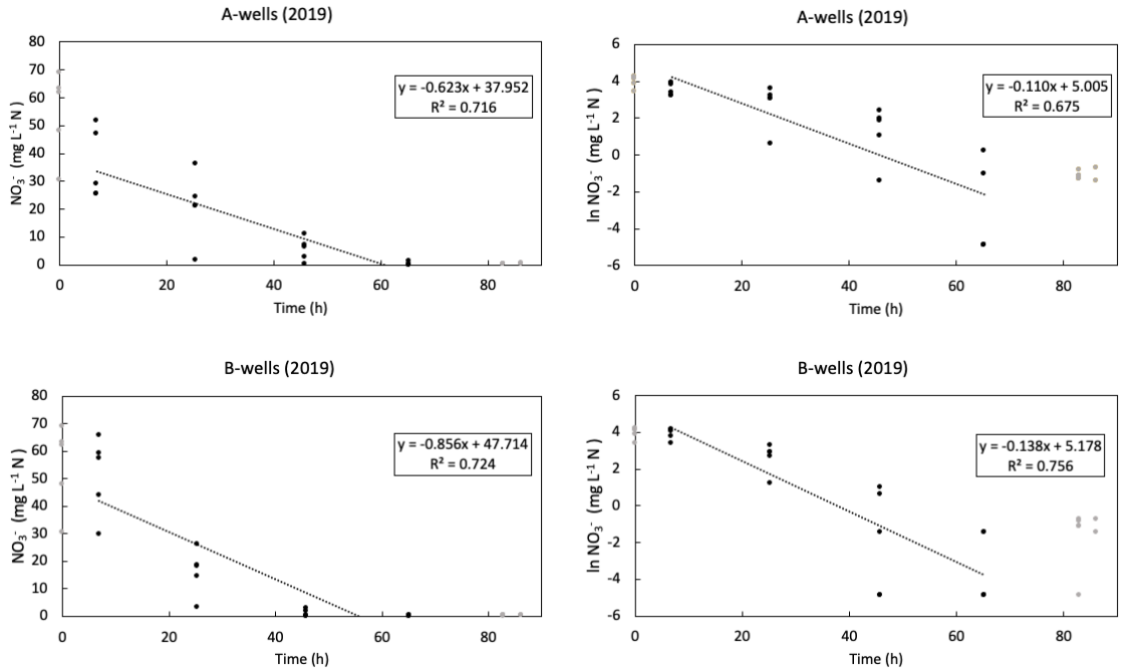

Figure E2. Graphical estimation for nitrates removal rates for the sampling profile of 2019 (grouping approach).

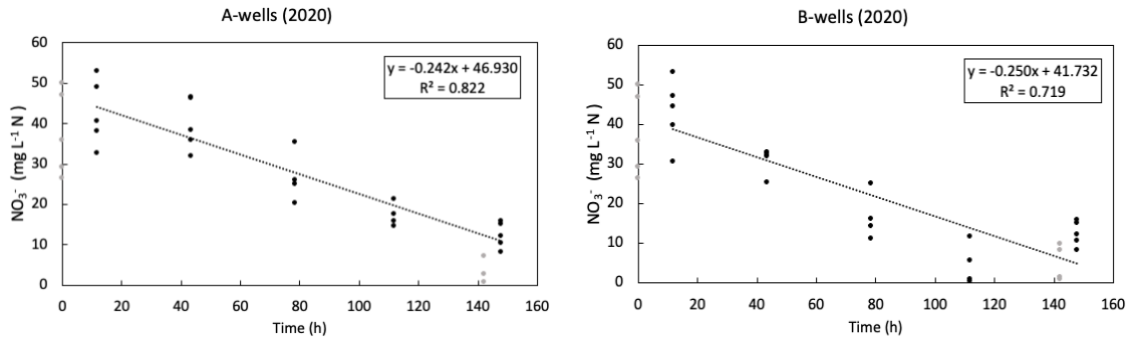

Figure E3. Graphical estimation for nitrates removal rates for the sampling profile of 2020 (grouping approach).

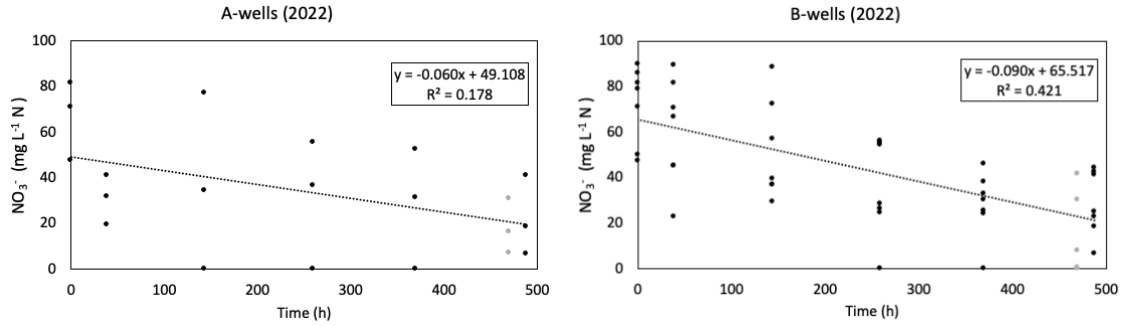

Figure E4. Graphical estimation for nitrates removal rates for the sampling profile of 2022 (grouping approach).

Table E2. Nitrate removal rates values obtained from graphical estimation by grouping approach.

Date	Wells	Temperature (°C)	N-removal rate (mg L^{-1} h^{-1})	R^2 (%)
2019	A	3.29	0.11	67.5
	B	3.29	0.138	75.6
2020	A	3.9	0.242	82.2
	B	3.9	0.25	71.9
2022	A	8.95	0.06	17.8
	B	6.51	0.09	42.1

E.3. Nitrate removal rates by individual approach

With the grouping approach, internal temperature and concentrations variations are not considered and an individual approach based on specific temperature becomes necessary. For 2019 and 2020, the temperatures were rather stable along the bioreactor distance since no heating device was installed. Therefore, some profile sampling results were considered together based on their according mean temperature (see appendix A, table A1) as seen in figure E5 and E6.

In contrast, 2022 presented high temperature variation along the distance and taking the mean value would have underestimated the actual temperature. The values from table A.4 were then plotted with the nitrate concentrations for each sampling profile and the nitrate removal rate graphical estimation was performed not only for each sampling profile but also within the profile itself. In general, temperature plateau (represented by temperature horizontal lines in the graphs) that had a decline in nitrate concentrations were used to define the limits to estimate the rates (figure E7). The 3rd of March was not considered since it showed the result of a mixing effect instead of the heating effect. All nitrate removal rates results are shown in table E3.

Finally, as stated before, 2019 mainly showed a better fit for the 1st order rate law while 2020 and 2020 were defined by a 0th order rate law.

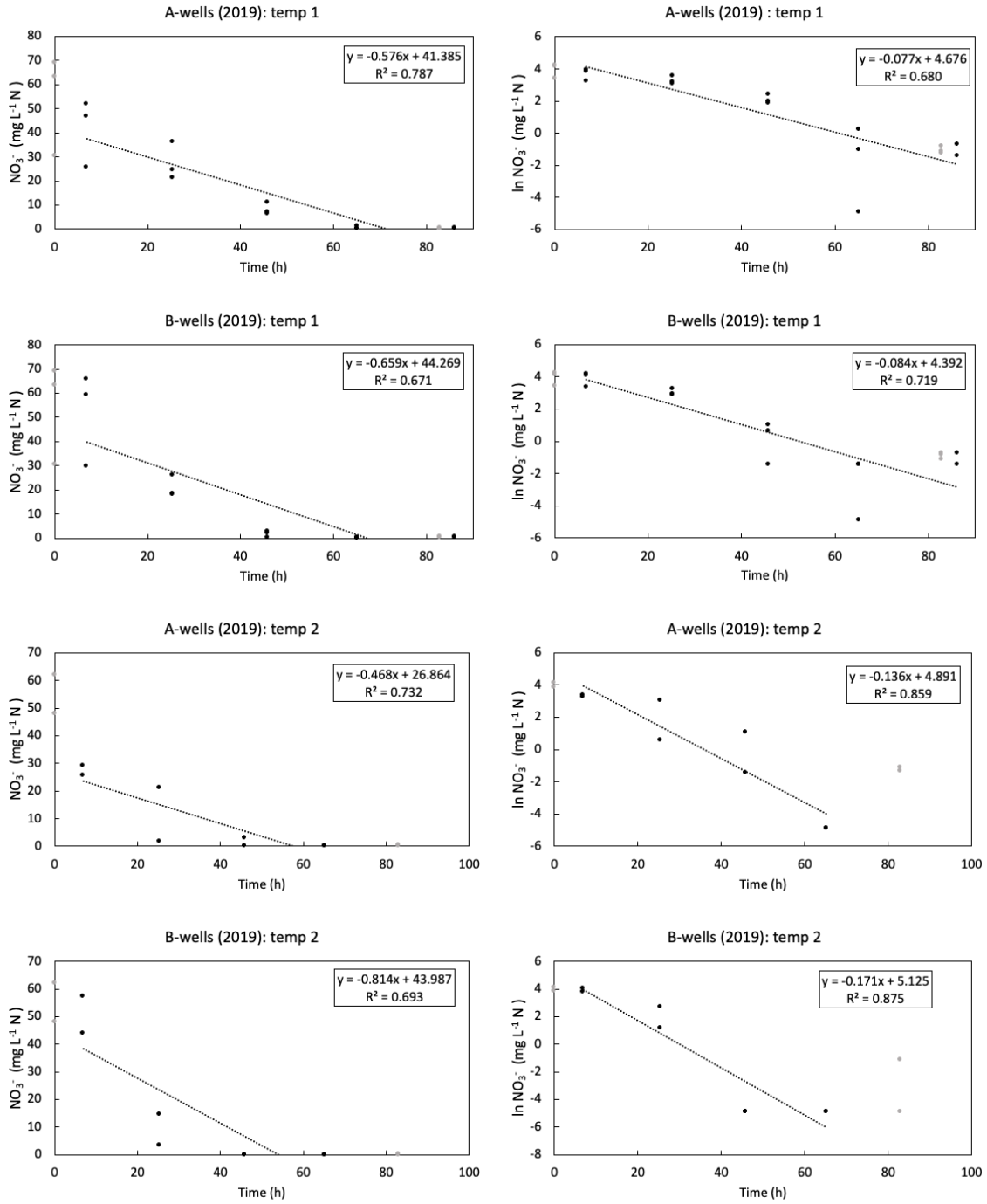

Figure E5. Graphical estimation for nitrates removal rates for the sampling profile of 2019 (individual approach). Temp 1 refers to 2.93°C for the 20th of June, 24th of June and 28th of July while temp 2 is for 3.83°C for the 2nd and 5th of July.

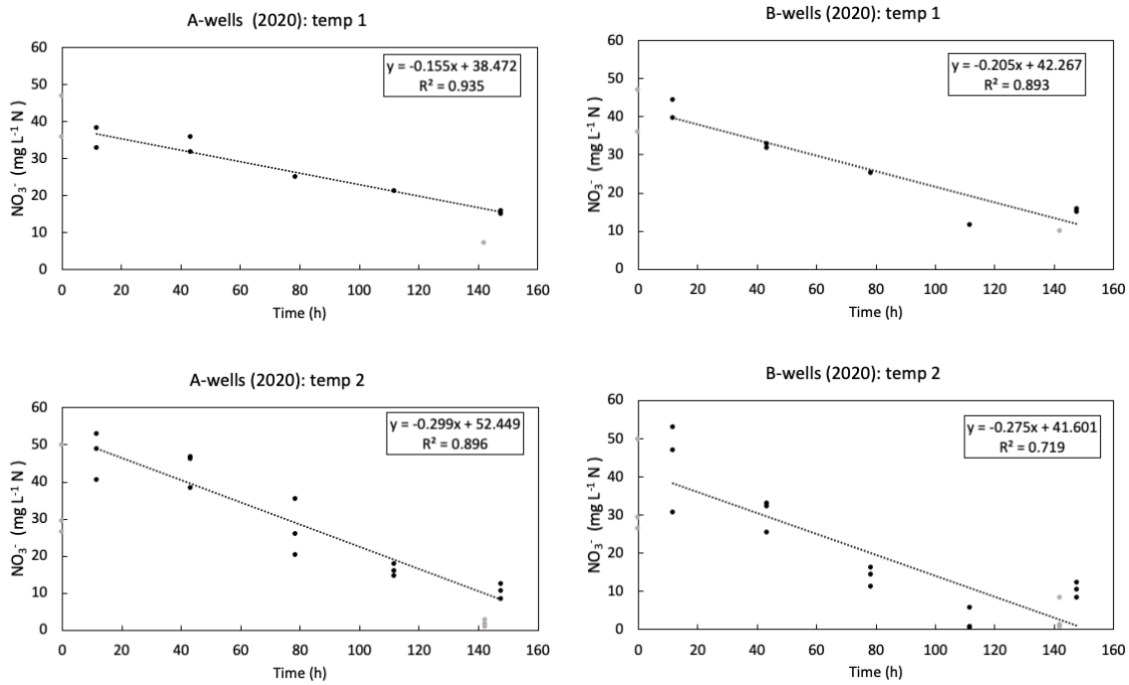

Figure E6. Graphical estimation for nitrates removal rates for the sampling profile of 2020 (individual approach). Temp 1 refers to 2.76°C for the 17th and 22nd of June while temp 2 stands for 4.6°C for the 29th of June, the 7th and 13th of July.

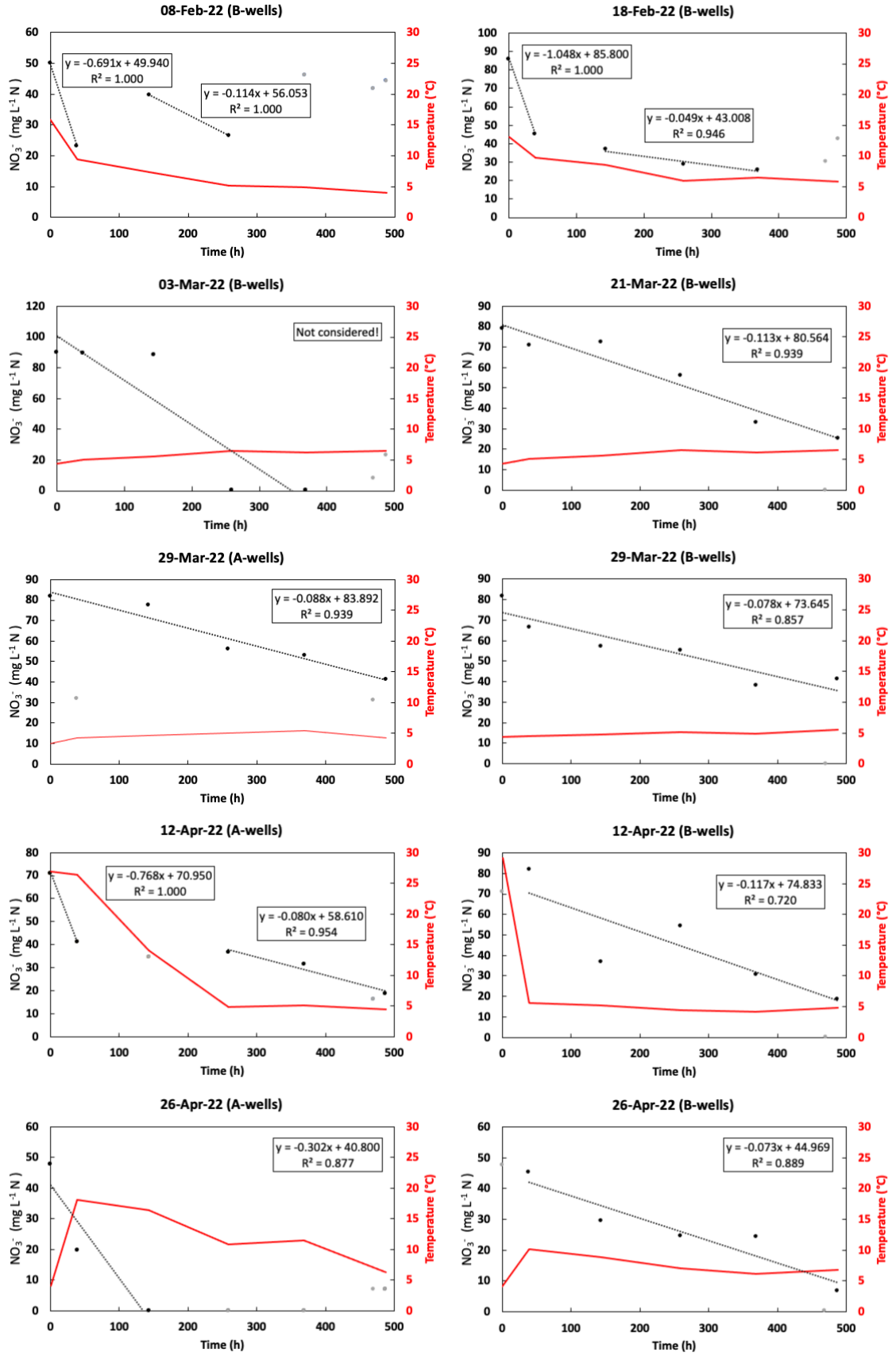

Figure E7 Graphical estimation for nitrates removal rates for the sampling profile of 2022 (individual approach).

Table E3. Removal rates values obtained from graphical estimation by individual approach. For 2019 temp 1 refers to the 20th of June, the 24th of June and the 28th of July while temp 2 is for the 2nd and the 5th of July. For 2020, temp 1 stands for the 17th and 22nd of June while temp 2 is for the 29th of June, the 7th and 13th of July. Overall the N-removal rate value are within the range found by a previous study on denitrifying woodchip bioreactor (1.4-35 g m^{-3} d^{-1} = 0.058-1.458 mg L^{-1} h^{-1} from temperatures at 15.5°C and 1.5°C (Feyereisen et al. 2016)).

Date	Wells	Temperature (°C)	N-removal rate (mg L^{-1} h^{-1})	R^2 (%)
2019	A (temp 1)	2.93	0.077	68.0
	A (temp 2)	3.83	0.136	85.9
	B (temp 1)	2.93	0.084	71.9
	B (temp 2)	3.83	0.171	87.5
2020	A (temp 1)	2.76	0.155	93.5
	A (temp 2)	4.6	0.299	89.6
	B (temp 1)	2.76	0.205	89.3
	B (temp 2)	4.6	0.275	71.9
29-Mar-22	A	4.49	0.088	93.9
12-Apr-22	A	26.65	0.768	1.0
12-Apr-22	A	4.78	0.080	95.4
26-Apr-22	A	15.20	0.302	87.7
08-Feb-22	B	6.25	0.114	1.0
08-Feb-22	B	12.61	0.691	1.0
18-Feb-22	B	11.39	1.048	1.0
18-Feb-22	B	6.97	0.049	94.6
21-Mar-22	B	5.07	0.113	93.9
29-Mar-22	B	4.82	0.078	85.7
12-Apr-22	B	4.73	0.117	72.0
26-Apr-22	B	7.55	0.073	88.9

Appendix F: Potential preferential flowpaths

The DBR flowpath was initially assumed to be homogenous and cover the entirety of the bioreactor. However, during the study period, it was observed that higher temperatures propagated faster in the shallow areas. A hypothesis that could explain this phenomenon is that flow velocity is unevenly distributed through the system. It seems that water travels faster in the shallow parts (figure F1, above).

Furthermore, well P5 showed unexpected values for almost all the chemical analysis performed and could suggest that the flowpath passes to the side of P5 to directly join the outlet on the side of the bioreactor (figure F1, below).

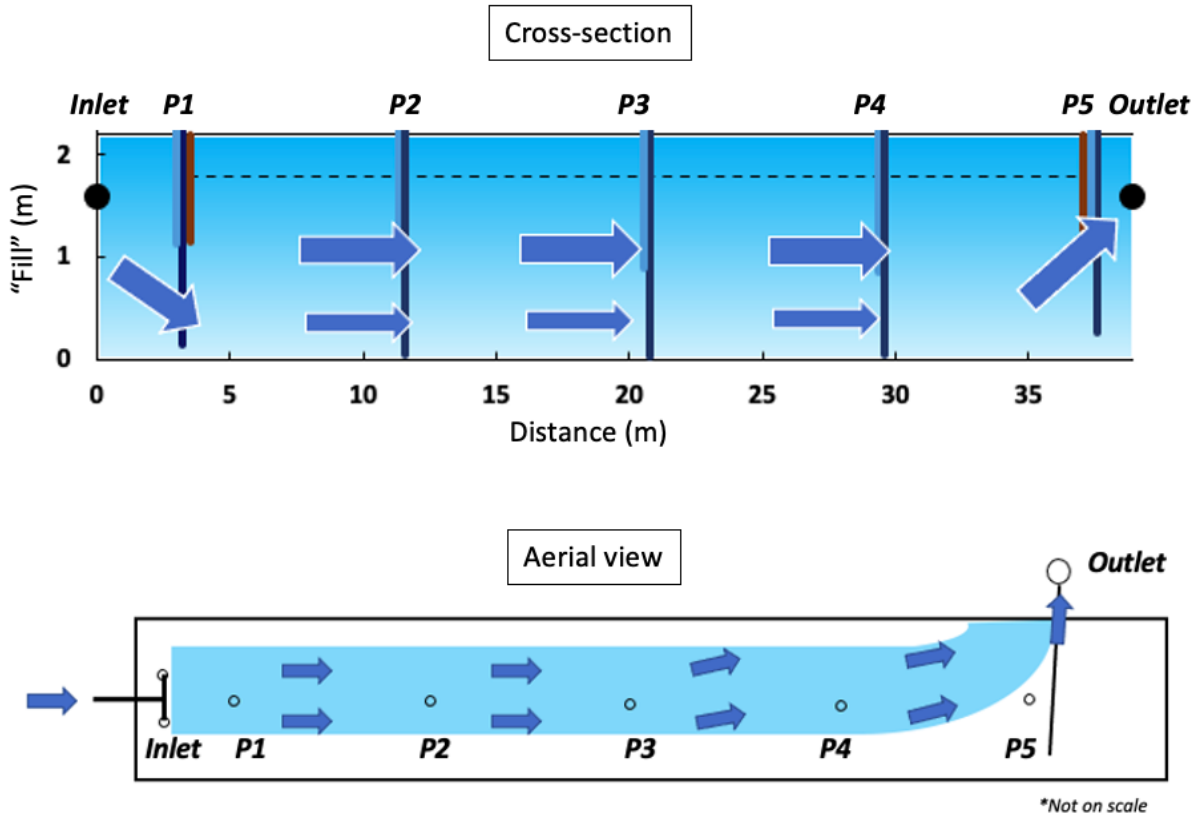

Figure F1. Potential preferential flowpath within the bioreactor: cross-section (above) and aerial view (below).

Examensarbete vid Institutionen för geovetenskaper
ISSN 1650-6553